TRIBHUVAN UNIVERSITY
INSTITUTE OF ENGINEERING
PULCHOWK CAMPUS

THESIS NO:

Sand Erosion in Francis Runner: A Case Study of Middle Marsyangdi Hydropower Station (MMHPS)

by
Prabesh Raj Devkota

A THESIS
SUBMITTED TO THE DEPARTMENT OF MECHANICAL AND AEROSPACE ENGINEERING
IN PARTIAL FULFILLMENT OF THE REQUIREMENTS FOR
THE DEGREE OF MASTER IN
MECHANICAL SYSTEMS DESIGN AND ENGINEERING

DEPARTMENT OF MECHANICAL AND AEROSPACE ENGINEERING
LALITPUR, NEPAL

AUGUST, 2020

COPYRIGHT

TRIBHUVAN UNIVERSITY

INSTITUTE OF ENGINEERING

PULCHOWK CAMPUS

DEPARTMENT OF MECHANICAL AND AEROSPACE ENGINEERING

The undersigned certify that they have read, and recommended to the Institute of Engineering for acceptance, a thesis entitled " Sand Erosion in Francis Runner: A Case study of Middle Marsyangdi Hydropower Station " submitted by Prabesh Raj Devkota in partial fulfillment of the requirements for the degree of Master in Mechanical System Design and Engineering.

_____

Supervisor, Dr. Laxman Poudel
Professor, Department of Mechanical and Aerospace Engineering, Pulchowk Campus

_____

External Examiner, Dr. Ishwor Bajracharya
Scientist, Nepal Academy of Science and Technology (NAST)

_____

Committee Chairperson, Dr. Nawraj Bhattarai
Head, Department of Mechanical and Aerospace Engineering, Pulchowk Campus

Date: July 2020

ABSTRACT

Middle Marsyangdi hydropower station (MMHPS) is situated in Siundibar, Lamjung and has an installed capacity of 70 MW. Sand erosion is one of the major problems faced by the station. Due to substantial presence of sand in the Marsyangdi river, the Francis Turbine components are hugely eroded, especially in the rainy season during the months of June, July and August. The runner is dismantled once every two years of continuous operation for overhauling and it was found that the eroded turbine components were the primary cause for MMHPS to bear huge financial losses due to maintenance activities as well as unit shutdown during overhauling. To prevent such losses, it is necessary to predict the erosion prone areas in the turbine components and necessary solutions like suitable coating are to be used for optimized performance and reduced financial and power losses. This study predicts the erosion prone areas of Francis runner at different wicket gate openings using the ANSYS CFX simulation software. The erosion analysis has been categorized into qualitative and quantitative analysis. The qualitative results from both simulation and actual data obtained during field visit were found to be of similar nature. The trailing edges of the runner blades were found to be mostly eroded. Leading edge erosion was found to be due to direct impact of sand-laden water emerging from guide vane opening and trailing edge side erosion was found to be due to high outlet velocity, pressure drop as well as curved runner profile. The quantitative measurement was performed at the site in which the reduction in blade thickness was measured. The erosion rate density from both simulation and site measurement have been compared. Elastomeric semi-soft coating applied in the runner blades were found to be effective for minimizing the sand erosion.

ACKNOWLEDGMENT

The research work on sand erosion in Francis runner has been a great opportunity for gaining fruitful insight on the matter. It is my radiant sentiments to place on record my best regards and deepest sense of gratitude to my project supervisor Prof. Dr. Laxman Poudel, who despite being extraordinarily busy with his duties, provided his valuable time to hear, guide, supervise and impart me with knowledge on various aspects of the research.

I hereby would like to express my profound sense of gratitude to Er. Atmesh Poudyal, Assistant manager, NEA who not only guided me but also gave me valuable suggestions and equipment needed for site visit. I indebted to the entire team of Middle Marsyangdi Hydropower Station (MMHPS) for their support.

My deepest sense of gratitude to Dr. Sailesh Chitrakar, Er. Dadi Ram Dahal and Er. Amul Ghimire who guided me throughout the entire stay at KU for Simulation analysis.

I also take this opportunity to highly acknowledge Assistant Professor Mr. Hari Dura whose selfless help and guides help me to achieve my objectives on this Research and to express my sincere gratitude to the entire department of Mechanical and Aerospace Engineering, Pulchowk Campus, for their cooperation, coordination and constant support to help me achieve my goals on this Research.

I pay my gratitude to Nipesh Regmi, Sudin Bhuju Shrestha, Alok Neupane, Sher Mohammad Hussain, Chiranjibi Acharya, Sanjaya Pathak, Pradeep Bartaula, Rajendra Dhakal, Ramesh Shrestha, Ashesh Babu Timalsina, and Neeraj Adhikari whose selfless time and technical support kept me going.

I would also like to thank the Hydro Lab team for testing the Sediment samples and providing the required results.

Lastly, I would like to pay my acknowledgment towards my family and friends for their continuous and unparalleled love, guide and showing all the way to perceive this opportunity. I consider their support a major backbone as I would be unable to achieve results without it.

TABLE OF CONTENTS

LIST OF FIGURES

LIST OF TABLES

LIST OF ABBREVIATIONS

Particular	Description
ATM	Automatic Topology Meshing
CFD	Computational Fluid Dynamics
FEM	Finite element Method
GV	Guide Vane
GWhr	Giga watt hour
HVOF	High velocity Oxy-Acetylene Flame
JHC	Jhimrukh Hydroelectric center
LE	Leading Edge
MMHPS	Middle Marsyangdi Hydro Power Station
MW	Mega Watt
NEA	Nepal Electricity Authority
PPM	Parts per Million
RPM	Revolution per minute
RV	Runner Vane
SST	Shear Stress Transport
TE	Trailing Edge

LIST OF SYMBOLS

Symbol	Description
B	Blade angle
E	Epsilon
m_p	Mass of particle
P	Density of turbine material
Ω	Omega
A	Guide Vane opening angle

CHAPTER ONE: INTRODUCTION

1.1 Background

Damages in hydraulic machinery are mainly caused due to the sediment erosion, cavitation, defects on material and fatigues. Wear is defined as the collective term for the different mechanism which cause deformation and displacement on solid surfaces. Wear in hydraulic machinery can be classified into two types.

a) Erosive wear

b) Abrasive wear

Erosive wear is caused by the collision of sand particles with the metal surface in which particles hit the surface with a certain velocity and angle and in abrasive wear a bed of particles slides over metal surface with velocity parallel with the metal surface and as a result material from surface gets removed by cutting (Stachowiak & Batchelor, 2001). Himalayan rivers hydropower plants are more prone to sediment and these sediments are more abrasive in nature that degrades the efficiency of the turbine. Sediments from these Himalayan Rivers either get deposited in the settling basin, reservoir, or passes through it. These both cases of sedimentation will affect hydropower plant operation, deposited sediment in the reservoir will decrease the capacity of reservoir thereby reducing the performance and production of the power plant and unsettled sediment passes through a tunnel that deteriorates turbine blades which also reduces power production. Hydropower plants should have an effective and efficient sediment handling system. Appropriate and efficient settling basin and flushing system of sediment help to increase the efficiency of the power plant and is one of the biggest issues in hydropower development of Nepal. Erosion, pitting, cavitation and corrosion are problems that degrade the efficiency of the turbine and sediment is the major particle that induces these problems. Sediment deteriorates turbine blades by removing material from its surface and changing its geometrical shape and is most prone in high head power plants. It is almost difficult to construct a power plant that completely prevents sediment to enter turbine section in high head sediment prone rivers. The rate of erosion in turbine surface largely depends upon physical properties of the sediment, chemical properties of sediment, and properties of turbine material and operating environment of power plant. Physical properties of sediments are its size, shape, hardness, concentration and roughness whereas chemical properties are its mineral

content and texture. Properties of turbine material are its elastic property, hardness, texture, morphology and chemistry whereas operating environment of power plant involves impingement angle, velocity, concentration, flow, temperature and pressure. In Nepal, it is found that Francis is the most eroded turbine blade as compared to others due to sediment. It may be due to the selection of such turbines for high and medium head power plants where sediment strikes turbine blades in high velocity in different angles. Not only such turbines, but a high concentration of sediment affects turbine that runs in low head like Kaplan and Propeller. It also erodes components associated with turbines like inlet valves, spiral casing, draft tube, wheel pits, faceplates, guide vanes, seal rings, needles and nozzle (Poudel, 2016).

Sand is a naturally occurring material having the composition of fine and divided particles. Looking the difference, sand and sediment differ slightly, sand consist of fine grains of rocks or minerals, mostly quartz fragments, found on rivers, soil whereas sediment is a naturally occurring substance that gets broken down by water, or ice or by force of gravity acting on the particles or it is a collection of small particles, dirt's, that precipitates from the river or other body of water (Poudel, 2016).

Sand can also be defined as a material made up of grains that are anywhere from .0625 millimeters to 2.0 millimeter in diameter. Furthermore, the minerals that make up sand are also important when it comes to defining sand. The most common mineral in sand are silica, quartz, mica and feldspar. Sediment can be classified in terms of its size, shape, mineral content, texture and hardness. It differs according to origin, earth's geology, chemical reaction, use and other factor likes wind, water transformation, and weather condition etc. (Poudel, 2016).

The scope of Francis turbine is broad in small and large hydropower plants. It is due to the geographical structure and head available. Nepalese river contains a bulk amount of sediment (silt and sand) especially in rainy season (Thapa, et al., 2005). Due to the presence of sediment particles, there is a wear and tear in turbine and its components. Sediment wear (Erosion) is defined as the loss of material due to contact between sediment particle and & solid material. Erosion is one of the major problems in Francis runner and its component. Bulk content of unsettled sediment particles flowing through the turbine and its components during rainy season erode the surface when comes in direct contact. The wear on turbine and its components depends upon various parameters such as size and shape of sediment particles, the impact velocity along with

impingement angle, the operational hour of turbine, its components and the material used in the turbines and its components (Noon, 2017). The higher the sediment content and the harder the minerals like quartz and feldspar having higher hardness value, greater is the wear and this will result in the poor performance of the plant than its optimal limit (Pradhan, 2004). Erosion in Francis turbine are predominant in GV's and runner blades and erosion mechanism in the turbine components depend upon the flow nature inside the turbine components (Gautam, 2019). The gradual removal of base material changes the profile of the turbine blades and its components and also weaken the structure, loss of turbine hydraulic efficiency, which in result loss of energy production and also leads to shut down the plant for repair and maintenance. In such condition, there will be loss in energy generation and cost occur for repair and maintenance (Noon, 2017).

Sand induced wear is a serious problem for run-off river power plants in Himalayas River in Nepal. Thermodynamic measurement carried out for a turbine in Jhirmuk Hydroelectric Centre (JHC) showed decrease in efficiency substantially due to sediment erosion (Pradhan, 2004). Looking the mineralogical distribution, the content of quartz and feldspar are more in Nepalese river. The mineralogical distribution done at Jhimrukh Hydroelectric Center (JHC) found that 60-65% of sediment consists of quartz and 20-25% of feldspar with Mohr's hardness of 6-7 (Thapa, et al., 2012). Looking the particle size diameter it was found that 90% of the particle entering the turbine are below 0.1mm in diameter and mean diameter entering the turbines are 0.025 in JHC (Thapa, et al., 2012).It is found that the concentration of sediment during peak monsoon ranges from 2000-6000 ppm and reach up to 60,000ppm (Pradhan, 2004). As looking the effect it will create alteration and change in blade profile, fatigue and damage of turbine and its components, increased vibration, inefficient operation, noise and final breakdown of turbine and its components (Padhy & Saini, 2008).

Figure 1.1: Eroded runner and guide vane of Kaligandaki HPS obtained during site visit

The problem of erosion cannot be completely removed but it can be decreased. Several methods and techniques have been developed and implemented to reduce the problem of erosion on hydraulic turbines and its components which includes

i) Prevention of sediment in the catchment area (Schleiss, et al., 2016)

ii) Tapping sediments at intake (using de-settling basins) (Pandit & shakya, 2018)

iii) Applying different type preventing coatings on the components which get exposed to high velocity water like HVOF, flame and ceramic-metallic putty (Shrestha, et al., 2013)

iv) Shutting down the power plant when there is an excessive amount of sediment load in intake especially in the rainy season (Bishwakarma & St{\o}le, 2008).

Numerous researches have been conducted on the sediment erosion of Francis turbines. Some studies performed a mathematical model for estimating the effect of sediment erosion. (Kang, et al., 2016) in his research developed an erosion model in order to express suitable design, operation, and maintenance plan for Francis runner and predicted the sediment erosion of Francis turbine runner using different operating conditions and found the pressure side and runner outlet side as an erosion prone area (Kang, et al., 2016).

1.2 An introduction to Middle Marsyangdi Hydropower Station (MMHPS)

Middle Marsyangdi hydropower station is situated in Siundibar, Lamjung with installed capacity of 70 MW and is a peak run-off the river type scheme with a five-hour daily pondage design annual generation of 398 GWh. The power house is located at a distance of about 170 km from Kathmandu and the headworks are located 8 km further away.

Table 1.1 Salient feature of Middle Marsyangdi Hydro Power Station (NEA, 2020)

Type	Run of river with daily poundage for 5 hours peaking
Location	Phalia Sanghu (Headworks) / Siudibar (Powerhouse)
Installed capacity	70 MW
Average annual generation	398 GWh
Catchment area	2,729 km2
Average annual flow	99.5 m3/s
Maximum gross head / Net head	110 m / 98 m
Dam	Combined concrete gravity and rock fill dam, crest length 95m
Number and Type	2 Francis, vertical shaft
Rated Discharge	40 m3/s
Rated output	35.9 MW
Rated speed	333.33 rpm

1.3 Problem Statement

Sand erosion is one of the major problems in hydraulic turbines. It is mainly because of the fact that most of the hydropower plants in Nepal are run-off-the-river type. During the rainy season, huge amount of sediment gets deposited on the turbine components and as a result substantial erosion occurs in the components. Sand mainly consist of quartz which has higher hardness than the parent material of turbine components which causes damage on the components the resulting effects are alteration of blade profile, increase in vibration, noise, inefficient operation and system failure. Numerous researches have been conducted for predicting the erosion pattern on Francis runner but there is insufficient study on quantitative measurement, i.e. erosion rate calculation. Flow simulations have been conducted but site measurement and comparison between the site measured result and simulation result have not been done sufficiently. This study wants to fulfill this gap by measuring the erosion rate using numerical analysis and comparing the site measurement result with numerical result so that it will be easier for predicting the erosion rate of Francis Runners, especially that of MMHPS to calculate the runner wear without dismantling it.

1.4 Objectives of Thesis

1.4.1 Main objective

To study the sand erosion on Francis runner of Middle Marsyangdi Hydropower station.

1.4.2 Specific objectives

- To perform the Qualitative and Quantitative analysis of MMHPS runner through field measurement.
- To predict the Erosion Pattern and erosion rate density using Simulation software ANSYS CFX.
- To compare the ANSYS simulation result (Erosion rate density) with the results obtained from the field visit.

1.5 Limitations

- The error analysis during the tracing of eroded area on the paper was not considered.
- The sediment concentration data of peak sediment containing month June, July and August was only considered.
- Coatings on the runner blades was not considered in the Numerical analysis
- Flow analysis was performed for single passage only.

CHAPTER TWO: LITERATURE REVIEW

2.1 Francis turbine terminologies

Hub: it is the upper side of the turbine where the shaft is attached.

Shroud: it is the lower side of the turbine, below the band as shown in figure 2.2.

Leading edge: it is the frontal edge of runner blade at the inlet through which water strikes the blade.

Trailing edge: it is the edge of the Francis turbine through which the water gets discharged to the draft tube

Pressure side: it is the side of the blade at which the incoming water strikes entering through the inlet.

Suction side: it is the opposite side than of the pressure side.

Crown: it is the upper wearing ring of the turbine as shown in figure 2.2.

Band: it is the turbine lower wearing ring as shown in figure 2.2.

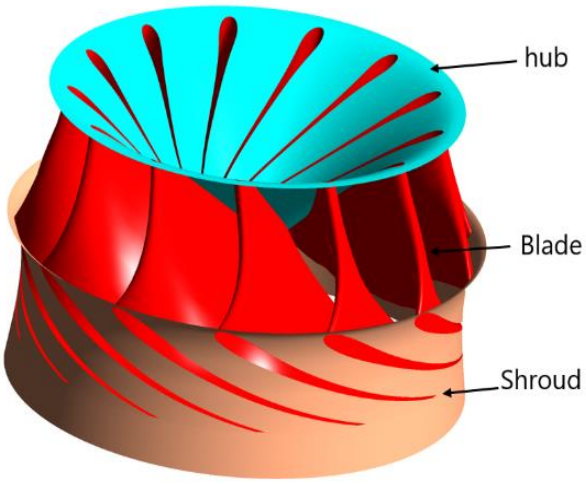

Figure 2.1: Nomenclature of designed runner on Bladegen

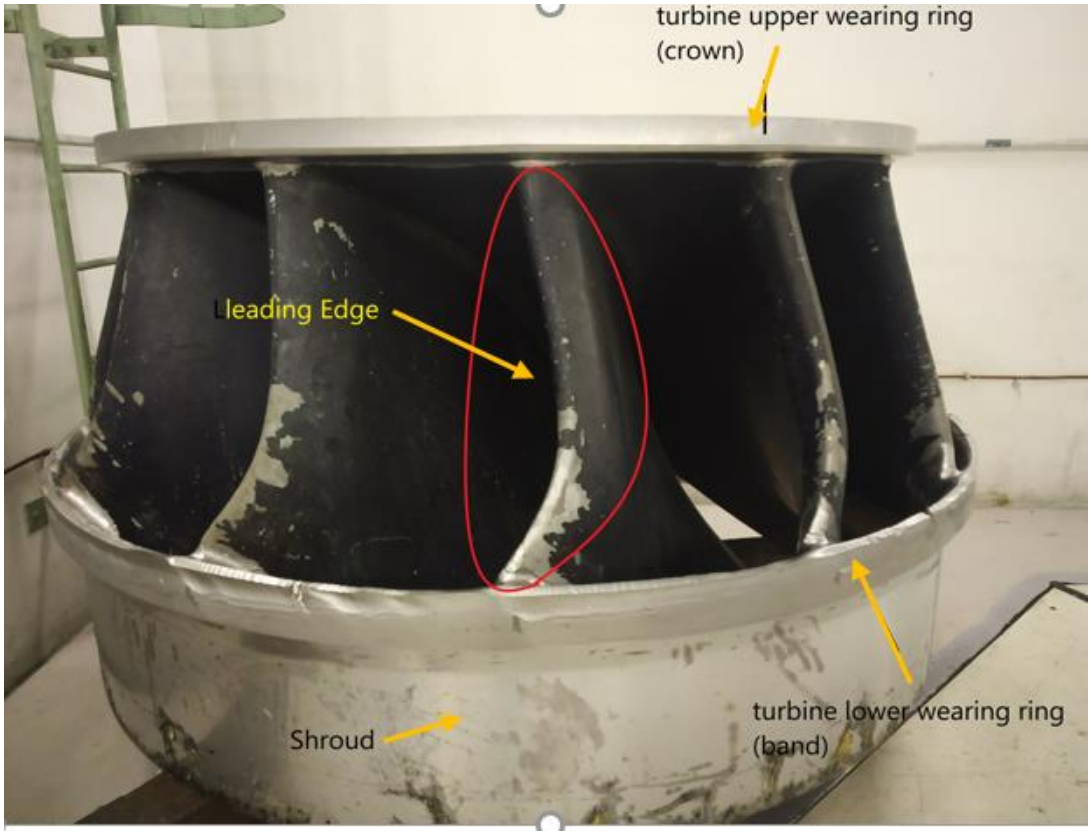

Figure 2.2: Nomenclature on photographed MMHPS runner

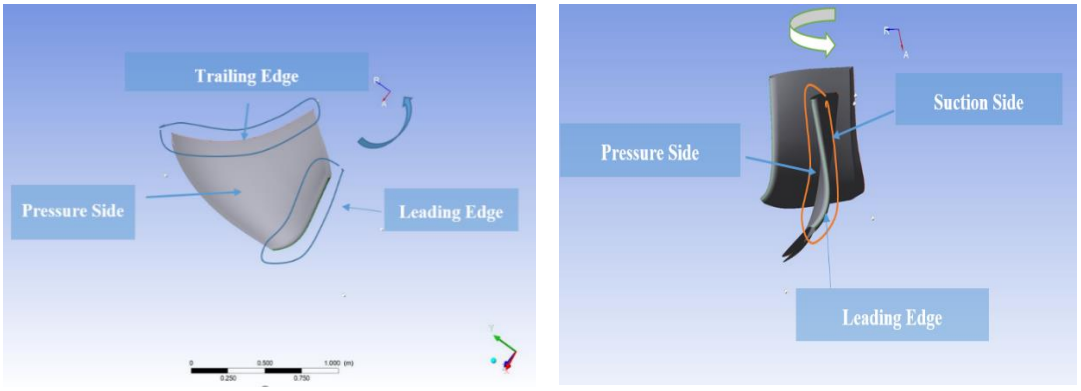

Figure 2.3: Nomenclature on designed blade

2.2 Overview of CFD

CFD is a computer-based tool and is used to simulate the fluid flow, especially in fluid mechanics and heat transfer problems. It is a branch of fluid mechanics which uses different numerical methods and algorithms to analyze the behavior of fluid and to solve the fluid related problem. It requires millions of calculations to simulate the fluid and gases interaction for solving different complex problems in science, engineering and medical sciences by using iterative process.in order to solve these problems, it will require high speed supercomputers for processing and may be time consuming.it is

suitable to perform the fluid flow analysis using CFD in smaller time with more accuracy especially for the analysis of flow type, nature and distribution of parameters. The solution methods in CFD are of different types. Finite volume and finite elements are the most commonly used amongst them.in finite volume method, the region to be analyzed is divided into small control volume. Now the equations are discretized for solving iteratively for each control volume. Another type is finite element method in which the region to be studied is divided into small no of elements and is widely used to analyze and solve the problem related to hydraulic machineries, stress and strain, dynamic response and eigenvalue analysis.

2.2.1 CFD structures

CFD software consist of sophisticated graphical user interface (GUI) for input problem and to examine the result. The components used are

- Pre-processing
- Solver
- Post-Processing

Pre processing

This is the early stage for analyzing problems and the activities performed at the preprocessing are:

- Geometry creation
- Mesh Generation
- Selection of physics and Fluid Properties
- Specification of Boundary Conditions

Solver

Solver is the main and important part of CFD analysis and is used to solve the flow related problem and to give the required result. Some common type of solver generally used are FLUENT, CFX and POLYFLOW. FLUENT and CFX are both developed by ANSYS independently having some similarities and difference too. CFX solver uses finite element to discretize the domain and fluent solver uses finite volume for domain discretization. The steps used to solve the governing equation of problem are

- Initialization
- Solution Control

- Monitoring Solution
- Monitoring Convergence (Regmi, et al., 2019)

Post processing

After using solver, the next step is to analyze the result using contour plots, vector plots streamline and rendering for graphical representation of the obtained result. The following results can be viewed.

- X-Y graphs
- Contour
- Velocity Vectors
- Data Report and Output
- Animation (Regmi, et al., 2019)

2.2.2 Turbulence Model

The generally used turbulence model in CFD analysis are as follows

- Standard k-ε model
- Standard k-ω model
- Shear-Stress Transport (SST) k-ω Model

The k-ε model is better for flow far from the boundary layer while the standard k-ω model is for flow near boundary layer. While the Shear-Stress Transport (SST) k-ω model was developed by Menter and is a newer and fidelity model used in turbo machinery. It combines the strength of both above models. It uses transformed versions of k- ε model far from the walls and k-ω model close to walls. Flow the problem of flow analysis on the runners, SST k-ω is one of the better option.it uses the flow near the boundary wall and away from the boundary wall as a result more accuracy in result is obtained. Due to these features' SST k-ω model is more accurate and reliable for flows like (e.g., adverse pressure gradient flows, transonic shock waves, airfoils than the standard k-ω model. (ANSYS, 2011).

2.2.3 Erosion Model

Two type of erosion model used generally in ANSYS CFX. One is Finnie erosion model and another is Tabakoff erosion model. Finnie erosion model computes the erosion in a surface by using kinetic energy of impacting particles. For almost all metals, erosion mainly depends on impact angle and velocity according to the relationship.

$$E = kV_p^n f(y) \quad 2.1$$

where, E is a dimensionless mass, V_p is the particle impact velocity and f (γ) is a dimensionless function of the impact angle. The value of the exponent, n is generally in the range 2.3 to 2.5 for metals. Choosing the value of n=2 makes this model compute the erosion from the kinetic energy of the impacting particle (ANSYS, 2006).

Tabakoff erosion model

$$\mathrm{E} = \mathrm{f}(\beta)\left(\frac{\mathrm{V_p}}{\mathrm{V_1}}\right)\cos^2\beta_1\left(1 - \mathrm{R}_\theta^2\right) + \mathrm{f}(\mathrm{V_{PN}}) \quad 2.2$$

$$f(\beta_1) = [1 + K_2.K_{12}.\sin\left(\beta_1.\frac{\pi/2}{\beta_0}\right)]^2 \quad 2.3$$

$$R_\theta = 1 - \frac{V_p}{V_3}.sin\beta_1 \quad 2.4$$

$$f(V_{PN}) = (\frac{V_p}{V_2}.sin\beta_1)^4 \quad 2.5$$

$$K_2 = 1\ if\ \beta_1 \leq 2\beta_0$$

$$k_2 = 0\ if\ \beta_1 > 2\beta_0$$

Erosion rate is expressed as the total amount of material loss per unit mass of impingement particles, R_θ is the tangential restituting factor, V_p is the particle impact velocity, β_1 is the impact angle in radians between the approaching particle and the surface and β_0 is the angle of maximum erosion.V_1, V_2, V_3 are the model velocity constant where $V_1 = \frac{1}{\sqrt{K_1}},\ V_2 = \frac{1}{\sqrt[4]{K_3}}, V_4 = \frac{1}{K_4}$

where, $\mathrm{K_1}, \mathrm{K_{2,}}\mathrm{K_3}$, $\mathrm{K_4}$ are the material constant having values $K_1 = 6.533 * 10^{-5}$, $\mathrm{K_{2,}} = 0.293328$, $\mathrm{k_3} = 6.44 * 10^{-11}$,$\mathrm{K_4} = 5.571 * 10^{-3}$.

Overall erosion rate due to a particle is calculated using formula

Erosion rate=E.N.m_p

where, N is the number rate and m_p is the mass of the particle (ANSYS, 2006).

2.3 Previous research and findings

The study performed on erosion wear on Francis turbine components due to sediment flow on tarbela dam hydel project in Pakistan and found that sediment particles has caused damage to the plant equipment like guide vane, stay vane, runner and draft tube. The prediction of erosion effect was done and found there was gradual removal of a runner and its component base material along with the change in profile and weaken in

structure. There was also the continuous loss of turbine hydraulic efficiency. The study concluded that erosion and efficiency loss will increase with the increase in sediment particle concentration and size (Noon, 2017).

The efficiency measurement of JHP was performed and found that 80% of hard minerals (Quartz +Feldspar) content is considered responsible for erosion. Also, the calculation was done to analyze the sediment load and found 6900 tons of sediment get passed through the turbine during the operational period of 3 months on the year 2003. The loss was found to be 4% at BEP and 8% at 25% load condition (Pradhan, 2004).

The case study of kaligandaki A HPS was performed and found that the content of quartz are higher in kaligandaki reservoir. The erosion on the leading edge and trailing edge tip and the guide vane was observed and concluded that the angle of guide vane largely affects the severity and localization of erosion phenomena (Koirala, et al., 2016).

Similar work was performed on the numerical study of sediment in which erosion pattern at different operating conditions and sediment inflow rate are studied. Simulation were conducted at different operating conditions and varying inflow rates of 1, 5, 10, 20, 30, 40, 50 kg/s and erosion pattern were found especially on the pressure side of the runner blade. As a conclusion, it was found that, with the increase in sediment inflow rate, the erosion rate increases almost in a linear manner and the main possible region of erosion are around the outlet of the runner (Kang, et al., 2016).

The study carried out on the methodology for the assessment of erosive wear on the Francis runner concluded that, there is severe wear due to the presence of hard minerals like quartz and feldspar. The analysis was performed using the model IEC-2013 including curvature effect and relative velocity. The average erosion rate was obtained and found to be 6.2mm in four year at the outlet side of the runner and agrees within 10% of actual site measurement. Also the erosive wear is severe at the outlet of the blade and it was due to high relative velocity (45.5m/s at the outlet) and (15.5m/s at the inlet) of power station located in India (Masoodi & Harmain, 2017).

A research conducted on review on silt erosion in hydro turbines concluded that, problem of silt erosion on turbine cannot be completely avoided but it can be reduced up to some extent by providing different materials and coatings to the turbine blades and suggested the necessity of further research and study of erosion on different flow conditions (Padhy & Saini, 2008).

Empirical modeling of sediment erosion in Francis turbine performed the selection of two erosion model to estimate erosion rate and consecutive efficiency reduction was analyzed. The study proposed the improved empirical relation for estimating erosion rate and validation was done by comparing with the experimental measurement at the site. This was the case study performed using improved erosion model of JHC and found the efficiency reduction by 1% per year. As a conclusion the obtained new erosion model can be used as an effective tool for formulating the appropriate design and maintenance strategy for the specific site Francis runner (Thapa, et al., 2012).

The research conducted on the analysis of sediment erosion of Francis turbine runner a case study in Himalayan region of India which focused on two hydropower (Uri and Dulhasti) located in Jammu and Kashmir and performed the analysis of sediment concentration and that at peak sediment season, the sediment concentration of the two rivers exceeds 5000ppm for Uri and 2500 ppm for Dulhasti. Looking the mineralogical analysis, the content of Quartz was high in both river (77%-79%) for Uri and (52%-55%) for Dulhasti. The analysis was performed using erosion model IEC-2013 and concluded that average erosion rate of 5.9mm in four year was found on Uri and 7.3mm per year for dulhasti (Masoodi & Harmain, 2017).

The PHD thesis performed on a study in sediment characterization and its impact on hydraulic turbine material classified the mineral content on the sand. Quartz, mica, feldspar, silica, clay, chlorites, dolomite carbonate are the content of the sand and among these, the most abundant sand content is Quartz. The classification of sediment according to size was also performed as sand lies in between the size of 0.0094 to 1.5 from very fine to very coarse. The thesis concluded that sand particles are the most abundant entity that degrades turbine efficiency by eroding material of the turbine and its components (Poudel, 2016).

2.4 Coating used in MMHPS Runner

Metaline series is an elastomeric coating product developed for customer-specific self-processing by spraying, casting or injection. The hardness is approximately 85 Shore A. The main field of application are wear protective coatings**.** Furthermore, suitable for the permanent repair or coating of rubber and metal component**s** to protect them from the most aggressive dynamic effects caused by impact, shock, wear and tear.

Table 2.1: Technical Specification of Elastomeric semi–soft protective coating obtained from MMHPS (MetaLine, n.d.)

Preferred usage	Wear, erosion and cavitation protection
Coating type	Elastomeric semi–soft protective coating
Consumption rate	1-1.25 kg/m^2 per 1mm thickness
Layer thickness	0.5 mm up to 3mm
Processing time at ambient condition	1-2 min
Solidification time	At 20°C, ≤ 2 days for no / light mechanical load
Hardness sprayed /cast on (A.S.T.M. D2240-68)	≥80Shore A
Tensile strength (A.S.T.M. D412-68)	≥20 N/mm^2
Tensile modulus at 100% elongation (A.S.T.M. D412-68)	≥7 N/mm^2
Tear resistance (DIN 53 515)	≥55 N/mm
Elongation at break (A.S.T.M. D412-68)	≥300 %
High temperature resistance (dry)	≥120°C
High temperature resistance (wet)	≥50°C
Low temperature resistance (dry)	≤0°C

CHAPTER THREE: RESEARCH METHODOLOGY

Firstly, the design of MMHPS Runner profile was performed using the bladeGen design software. After performing the design, the erosion rate density was determined using Flow Simulation in ANSYS CFX software. The study also includes field visit in which the Qualitative and Quantitative measurements were done and the results so obtained were compared with the simulation result. The steps involved in the determination of Sand erosion of Francis turbine in MMHPS runner are as follows.

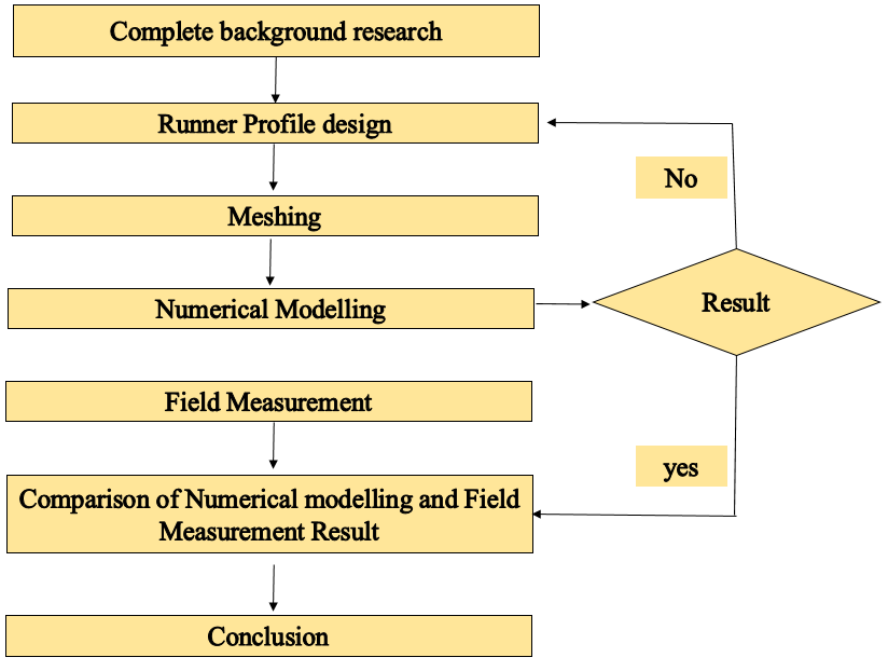

Figure 3.1: Methodology of the Research

3.1 Complete background research

Firstly, complete background research was performed and the problem due to erosion in Nepalese hydropower, especially in Francis turbines was studied. Previous researches and studies performed on sediment erosion and its remedies were studied. The related works on the previous research and findings were used giving the necessary references.

3.2 Runner Profile Design

The generation of the fluid domain for these types of analysis is always a challenge and toilsome work as the runner are already optimized and the hydraulic drawing is almost impossible to get. So, there are two possible solutions to this problem: 3D scan of the

physical model or conversion of available manufacturing drawing into the required format. However, it is almost impossible to carry out 3D scan of the model due to the unavailability of the precise scanner. That's the reason why the fluid model is created from the manufacturing drawings using AutoCAD and bladeGen.

First of all, manufacturing drawing is converted to CSV file using AutoCAD where the model is adjusted in 1:1 scale and the coordinate system is made similar to the bladegen format which can be observed in figure 3.4. After that the curve file is translated to bladeGen compactable format using excel and is imported in the bladeGen. Subsequently, the blade angle is measured from the available drawing which provides the information about the blade distribution which then is adopted in the bladeGen angle distribution. The distribution is made as close as possible by looking at the numerous snaps of the physical runner which are taken from all the possible positions. Again, bladeGen have features to control the blade thickness from one streamline to another streamline starting from hub toward shrouds wherein this thickness is also traced from the original drawing. Furthermore, for closeness lean angle is varied so to match the original turbine.

The process involved in designing the required runner geometry of the runner is shown in the flow diagram below in figure 3.2. The final domain from bladeGen and the runner snap can be seen in figure 3.3.

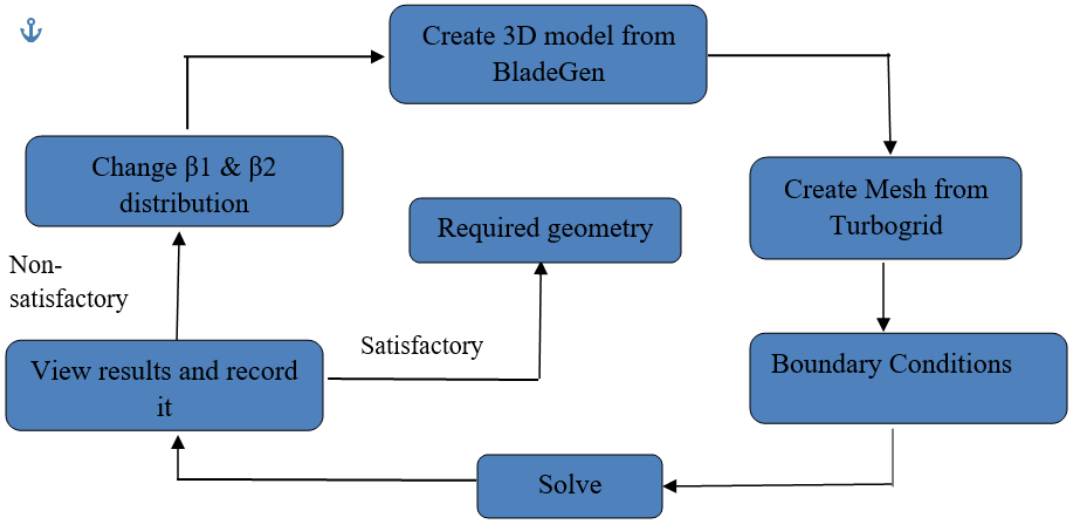

Figure 3.2: Process flow diagram of the Runner design

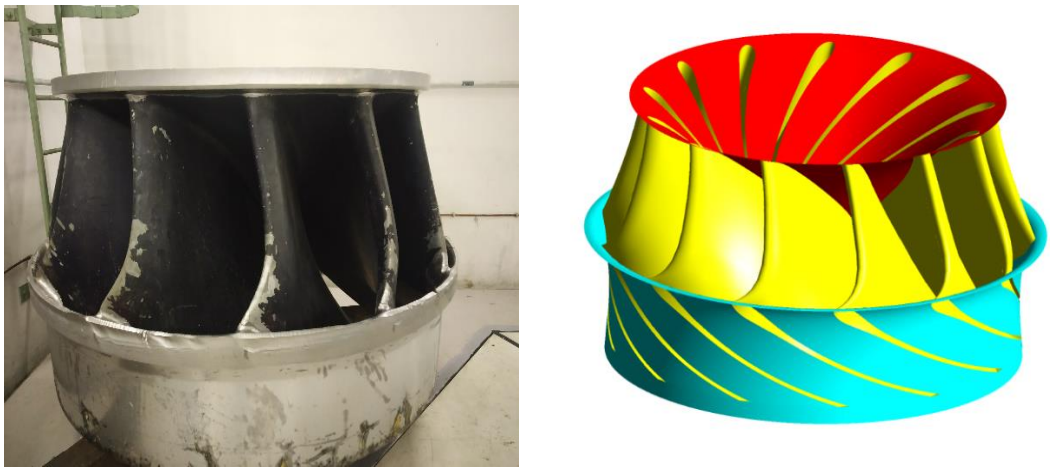

(a) (b)

Figure 3.3: (a) Actual MMHPS Runner (b) Designed MMHPS Runner in bladeGen

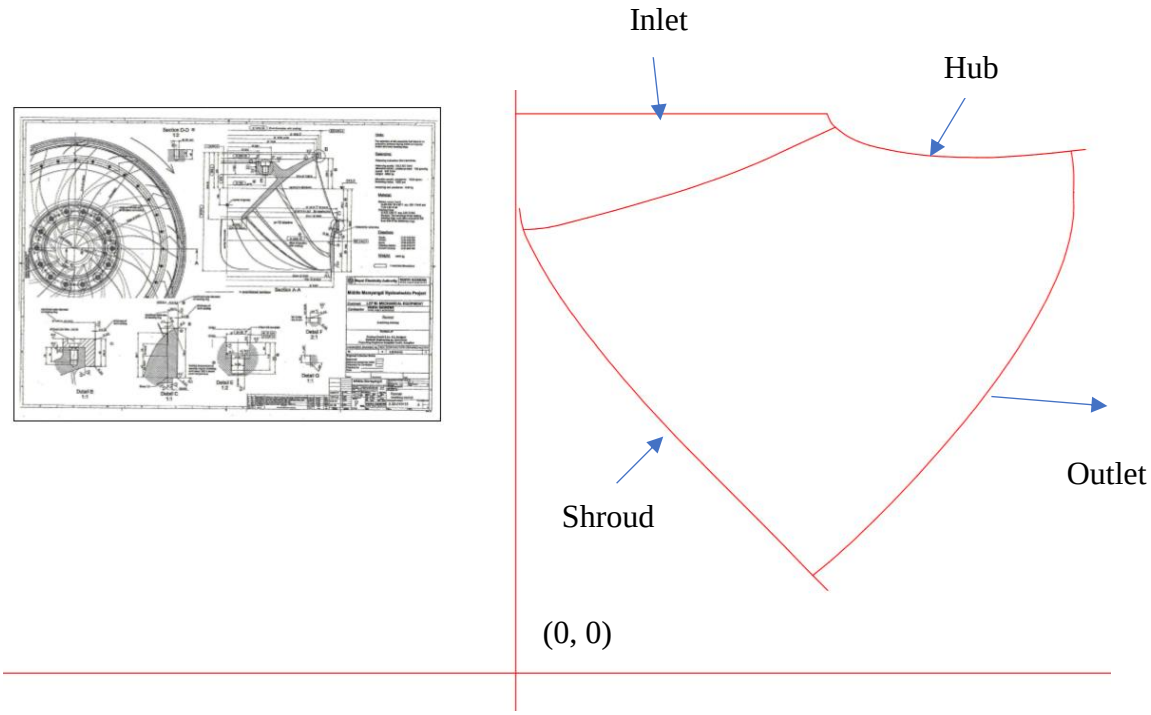

Figure 3.4: Tracing of MMHPS 2D drawing in AutoCad

3.3 Meshing

The optimized geometry obtained from the bladeGen is now imported in the Turbogrid for meshing which is then meshed by using the Automatic topology Meshing (ATM) method. The mesh independence test was performed and 0.61 million of elements were chosen for the meshing. Since a very large number of mesh elements are needed to simulate the Francis Turbine the domain with a single passage was created that has a blade in the middle. The calculation in the domain with the whole turbine comprising

all the necessary components would increase the computational cost as it would take a huge amount of time and require a very powerful computer. Even simulating in the domain with all thirteen blades would be costly in time. The turbine is rotationally periodic and simulating in only one passage is enough to visualize the flow and erosion rate density in the whole runner. The process involved are as follows:

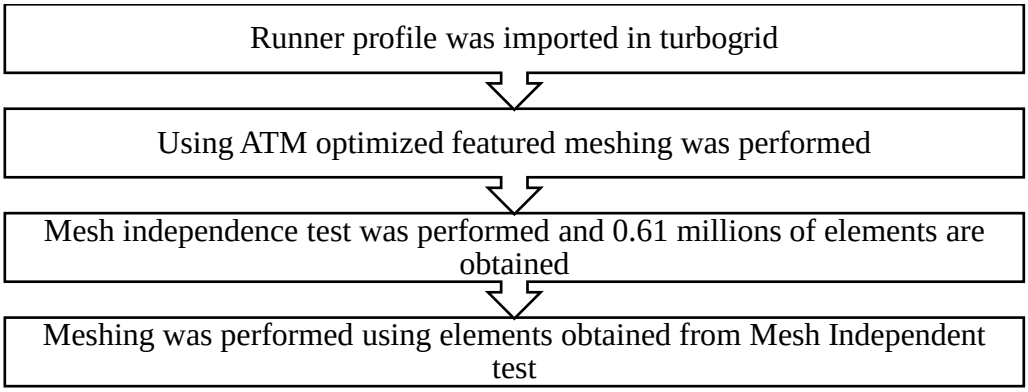

Figure 3.5: Steps involved in the meshing of blade domain

Turbogrid is the module for meshing the geometry especially for Turbomachinery which utilizes further processing the calculations in CFX. Turbogrid facilitates with options of several ways for the production of very good structured Hexahedral mesh of turbo-machineries. Automated method and Semi automated with lots of control over the mesh quality especially for turbomachinery are made available.

3.3.1 Mesh generation

The runner profile is now imported in the Turbogrid for mesh generation. For the generation of mesh, ATM optimized featured in Ansys Turbo Grid was used. An O-grid tropology was used to have a controlled transition to the inflation layer.

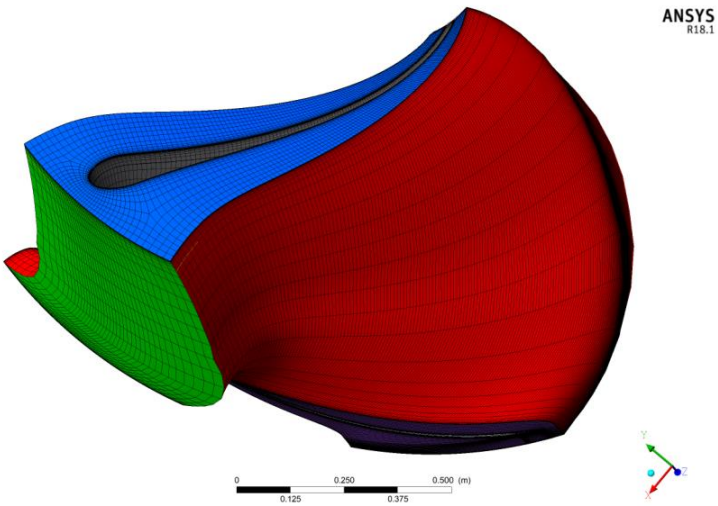

Figure 3.6: Mesh generation in blade domain

3.3.2 Mesh independence test

Mesh independence test was carried out for different mesh using the target passage mesh size and specifying the node count and giving target value. Boundary layer refinement control is proportional to mesh size. The factor base and factor ratio are used as a parameter to control the number of elements and for the better mesh quality maximum expansion rate of 1.3 is taken. For the different element number, the target value is varied through 50000 to 800000 and torque was considered as the parameter of interest during the test. After the mesh independence analysis, 0.61 million elements were chosen for analysis. The x-axis shows the number of elements in millions and the vertical axis shows the torque value in Joule.

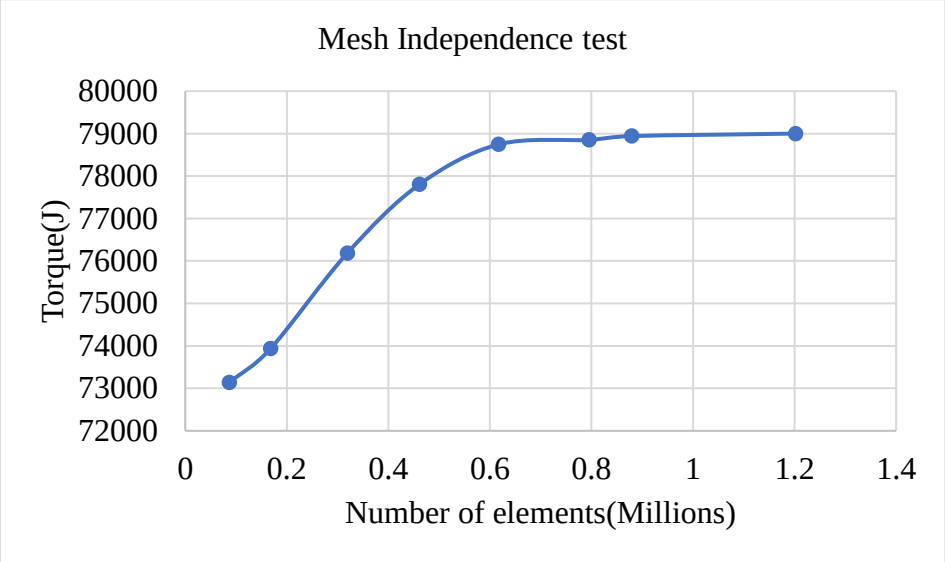

Figure 3.7: Mesh independence test

3.4 Numerical Modelling

Problem Definition in CFD

In this setting of analysis type, the required boundary condition, selection of required turbulence model along with erosion model will be defined.

i. Erosion model

ANSYS CFX generally consist of two erosion model: Finnie erosion model and tabakoff erosion model. The tabakoff erosion model is generally preferred over Finnie due to better control of variable of sediment and control structure. The parameters used in tabakoff erosion model are wider with better accuracy than Finnie. Due to these reasons tabakoff erosions model was preferred.

ii. Choosing the Turbulence model

The k-ε model is preferred better for flow far from the boundary layer and the standard k-ω model near for the boundary layer. Shear Stress Transport (SST) consist of the mixing of both and especially it is preferred for the flow over hydraulic machinery .in Francis turbine runner the flow of water occurs both near the wall and far from the wall in the blade surface and the hub shroud surface. So, it is preferable to use shear stress transport (SST) model for this simulation analysis.

iii. Boundary conditions

Running Simulation on CFX

The above boundary conditions are used in the CFX pre. The CFX solver then solve s the problems to give the result. The result thus obtained is analyzed in the CFX post to view the velocity distribution, pressure distribution and erosion rate density as required. The flow simulation was performed in ANSYS CFX. After performing meshing, using different flow angles and discharge values including different flow conditions, the flow simulation was performed. All the necessary data were obtained through drawing and the ANSYS CFD analysis. The detail stepwise process of simulation is as follows:

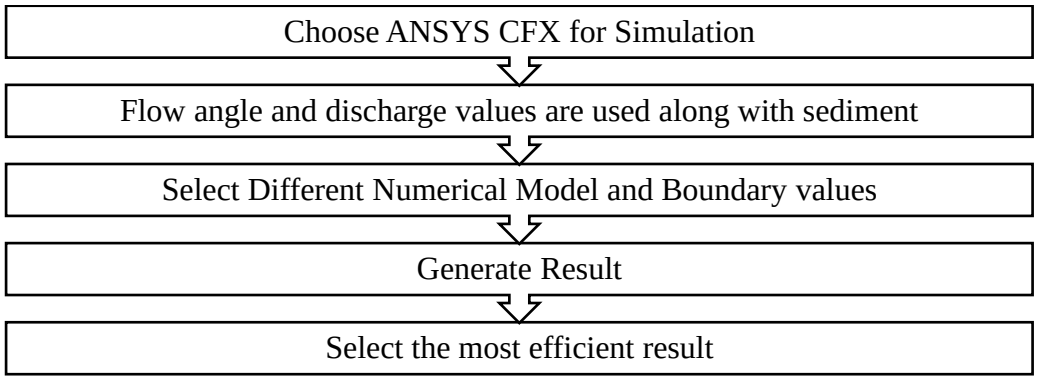

Figure 3.8: Different process involves in Flow simulation in ANSYS CFX

3.5 Determine guide vane opening angle and corresponding discharge

To determine the flow direction and velocity components, first the guide vane opening angle was determined. For this hill chart from the MMHPS drawing was used. The guide vane opening angle was found to be 32^0 at the fully opened condition with the full discharge of 40 m^3/s and fully closed at 0^0. Three operating conditions are considered and calculations are done.

Table 3.1: Gate opening and discharge value calculation

S N	Gate opening	Guide vane opening angle(α)	Discharge(m^3/s)
1	100%	32^0	40
2	75%	24^0	30
3	50%	16^0	20

3.5.1 Direction and flow magnitude calculation

From the design of Francis runner

$$Q=K\pi BDV_f \quad 3.1$$

where,

Q=discharge

K= factor which allows for the thickness of the vanes

B=width of the blade

D= outer diameter of the runner

V_1=velocity of jet at inlet

V_f= radial velocity

V_θ= tangential velocity

Now,

Diameter of Runner (D) =2256 mm

Width of the blade inlet (B) =635.8mm

Discharge (Q) =40 m^3/s

From the equation we get V_f=8.876 m/s

Now considering the velocity triangle on the inlet side of the Francis runner

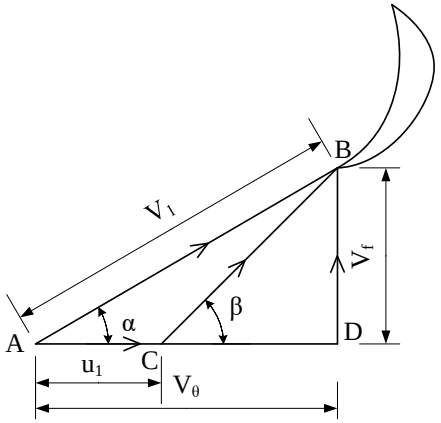

Figure 3.9: Velocity triangle at inlet side of Francis turbine

At full gate opening

Guide vane opening angle α= 32^0

From triangle ABD

Tan32^0=V_f/v_θ

v_θ=16.14 m/s

Now, total velocity

$$V_1=v_f e_r + v_\theta e_\theta \quad (3.2)$$

$$V_1=\sqrt{v_f^2 + v_\theta^2} \quad (3.3)$$

V_1=18.41 m/s

Now,

$$\overrightarrow{V1}=\frac{v_f}{|V1|}\widehat{e_r} + \frac{v_\theta}{|V1|}\widehat{e_\theta} \quad (3.4)$$

By solving the equation 3.4 we get

Radial component (r) = 0.481

Tangential component (θ) =0.876

Since the axial direction cosine =0 (radial turbine)

The flow velocity will be

(v_x) =0

(v_f) =8.876 m/s

(v_θ) =16.146 m/s

Similarly, we can calculate the direction cosine and velocity components at different guide vane opening angle by changing the value of α. The flow directions and velocity components at Best efficiency point and part load condition are shown on the table 3.2.

Table 3.2: Flow direction and velocity components at different gate opening

Load condition	Guide vane opening angle(α)	Flow Component		Velocity components (m/s)	
Full load (100%)	32	Axial	0	Axial (v_x)	0
		Radial (r)	0.481	Radial(v_f)	8.876
		Tangential (θ)	0.876	Tangential(v_θ)	16.146
75% load	24	Axial	0	Axial (v_x)	0
		Radial (r)	0.368	Radial(v_f)	8.876
		Tangential (θ)	0.929	Tangential(v_θ)	24.103
50% load	16.5	Axial	0	Axial (v_x)	0
		Radial (r)	0.24	Radial(v_f)	8.876
		Tangential (θ)	0.96	Tangential(v_θ)	34.56

3.6 Simulation Analysis portion

3.6.1 Flow simulation

After performing the Meshing in Turbogrid, the flow simulation was performed. Quartz and Water were used as particle and fluid for the simulation with Particle Transport Fluid Morphology. The diameter of the quartz used was 100 microns. Two different domains with stationary and rotating options were used. The fluid domain was stationary and the blade with hub and shroud was rotating domain with an angular velocity of 333.33 rpm. Reference pressure of 1 atm was used. The turbulence model used was Shear Stress Transport (SST) with an automatic wall function. The Tabakoff erosion model was used for Quartz with K12 constant of 0.585 and Reference Velocity 1, Reference Velocity 2, Reference Velocity 3 and Angle of Max. Erosion of 159.11, 194.75, 190.5 and 25 degrees respectively. One-way coupling between water and quartz was used with the Schiller Neumann drag force option.

3.6.2 Parameters investigated and boundary conditions used

The parameters and boundary condition used during the flow simulation is shown in table 3.3 below.

Table 3.3: Parameters and boundary conditions used for the flow simulation

Analysis type	Steady state analysis
Fluid and Particle definition	Water, Quartz
Inlet pressure	1062705 Pa
Outlet pressure	101325 Pa
Erosion model	Tabakoff erosion model
Eroding material	Quartz
Average diameter of Quartz	0.1mm
Shape factor	off
Turbulence model	SST model
Drag force	Schiller Neumann
Flow direction	Cylindrical components for sand also
No of positions	5000
Mass flow rate of Quartz	40kg/s
Convergence criterion	0.0001 residual
Wall function	automatic
Turbulence	Medium (Intensity = 5%)
Blade, Hub and Shroud (Rotating)	Boundary Type: Wall No slip and smooth wall

3.6.3 Workflow of Simulation

After designing the Runner in Bladgen, Turbogrid was used for the meshing, a mesh dependency test was performed without using the value of sediment. The optimum number of elements obtained through the dependency test was now used for the flow simulation using sediment value. The flow simulation was performed for a full load, BEP and part load condition which is shown below in the figure 3.10.

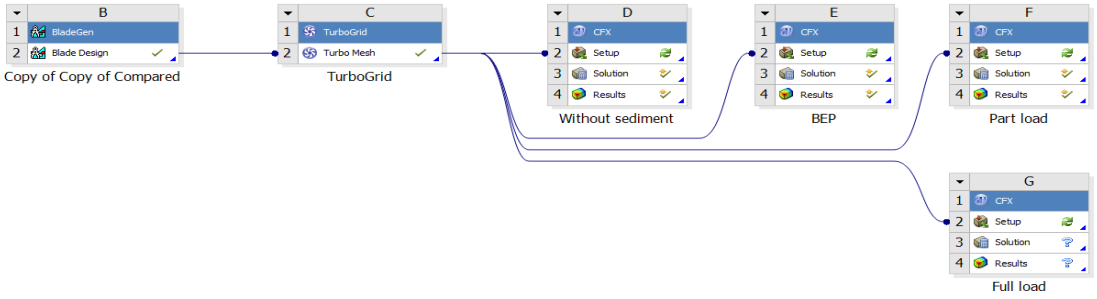

Figure 3.10: Workflow of simulation analysis

3.7 Field Measurement

All the necessary measurement was performed in MMHPS site during the period of Overhauling. The measurement was classified into two portions

a) Qualitative measurement

b) Quantitative measurement

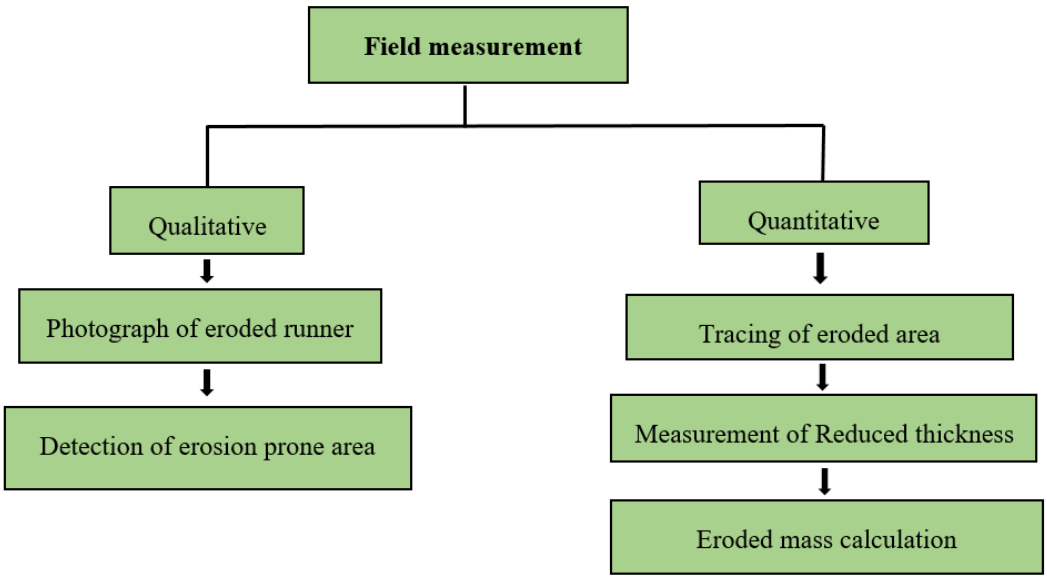

Figure 3.11: Different process involved in the Field measurement

In qualitative measurement, the photograph of the eroded runner was taken. The erosion prone area was detected from the photograph taken.

In quantitative measurement, transparent paper was used for the tracing of eroded blade of runner. Assuming small rectangular sections, eroded area was obtained. Now Vernier caliper was used for the measurement of reduced thickness on the trailing edge of blade. For the leading-edge erosion, the length and breadth of the eroded volume was calculated using measuring tape and for the depth, Vernier height gauge was used. The

eroded depth was measured at different section and average depth was considered for the analysis.

3.8 Comparison of results

The result obtained through the Numerical analysis and filed measurement was compared. The validation of the result was done by comparing the qualitative results obtained through the numerical analysis and filed measurement (photograph) and the comparison process are shown below.

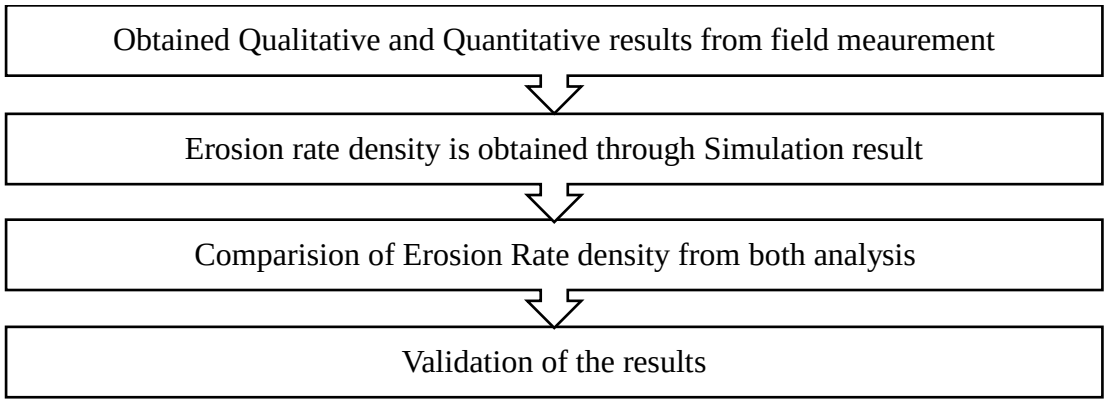

Figure 3.12: Process involving in Result comparison

3.9 Uncertainty analysis

Uncertainty analysis is the one of the mathematical models for error analysis under experimental section. Under the measurement of wear in Francis runner, the Vernier caliper and measuring tape was used for measurement of wear on leading and trailing edge of the blade. The length, breadth and depth were measured for calculating the eroded volume and by multiplying the eroded volume with density of turbine material, eroded mass was calculated. Therefore, Eroded volume is the function of length, breadth and depth. The least count of measuring tape was 1mm and the least count of Vernier caliper was 0.02mm while measuring the eroded volume. The details calculation part of error analysis is explained below.

V = f (l, b, d)

$$\sigma_v = \pm \sqrt{(\frac{\partial v}{\partial l}\ \sigma_l)^2 + (\frac{\partial v}{\partial b}\ \sigma_b)^2 + (\frac{\partial v}{\partial d}\ \sigma_d)^2} \quad 3.5$$

Where,

σ_v = Standard deviation of volume measurement

σ_l = Least count of measuring tape while measuring the length

σ_b = Least count of measuring tape while measuring the breadth

σ_d = Least count of Vernier caliper while measuring the depth

l= Length of eroded volume

b= Breadth of eroded volume

d= Depth of eroded volume

As we know that,

$\frac{\partial v}{\partial l}$ = (b×d)

$\frac{\partial v}{\partial b}$ = (l×d)

$\frac{\partial v}{\partial d}$ = (l×b)

$\sigma_v = \pm \sqrt{\{(b \times d)\sigma_l\}^2 + \{(l \times d)\sigma_b\}^2 + \{(l \times b)\sigma_d\}^2}$

$\sigma_v = \pm \sqrt{(1 \times 30 \times 10)^2 + (1 \times 50 \times 10)^2 + (0.02 \times 50 \times 30)^2}$

$\sigma_v = \pm 583.86$

Similarly, the error was calculated for all the thirteen number of blades. The error calculation done in table was of uniform type of erosion in the leading edge of the blade. The average error percentage obtained from the measuring instrument was found to be 3.89%.

Table 3.4: Instrument error calculation of the wear calculation on leading edge

Blade No	Length (mm)	Breadth (mm)	Depth (mm)	Volume (mm^3)	Error	%Error
1	50	30	10	15000	583.86	3.89
2	50	30	10	15000	583.86	3.89
3	50	30	10	15000	583.86	3.89
4	50	30	10	15000	583.86	3.89
5	50	30	10	15000	583.86	3.89
6	50	30	10	15000	583.86	3.89
7	50	30	10	15000	583.86	3.89
8	50	30	10	15000	583.86	3.89
9	50	30	10	15000	583.86	3.89
10	50	30	10	15000	583.86	3.89
11	50	30	10	15000	583.86	3.89
12	50	30	10	15000	583.86	3.89
13	50	30	10	15000	583.86	3.89
				Average Error		3.89

Table 3.5: Instrument error calculation of local wear at leading edge

Blade No	Length (mm)	Breadth (mm)	Depth (mm)	Volume (mm^3)	Error	%Error
1	46	22	5	5060	255.75	5.05
5	26	17	7	3094	217.63	7.03
8	50	32	6	9600	357.61	3.72
13	37	28	5	5180	232.92	4.49
				Average error		5.07

Similarly, the error was calculated for local large wear on the leading edge. The local large wear is detected is some blade only and the average error percentage was found to be 5.07%.

Table 3.6: Instrument error calculation on the trailing edge wear calculation

Blade No	length(mm)	Breadth (mm)	Depth (mm)	volume(mm^3)	Error	% Error
1	550	210	3.3	381150	3018.37	0.79
2	430	380	4.5	735300	4165.11	0.56
3	600	350	3.35	703500	4801.54	0.68
4	230	440	3.45	349140	2651.51	0.75
5	350	230	5.6	450800	2844.75	0.63
6	390	280	3.5	382200	2755.62	0.72
7	530	150	4.5	357750	2944.81	0.82
8	230	300	2.1	144900	1592.03	1.09
9	480	195	2.4	224640	2247.33	1.00
10	600	332	3.8	756960	4760.49	0.62
11	320	176	4.9	275968	2114.50	0.76
12	290	430	3.1	386570	2967.34	0.76
13	330	300	2.9	287100	2364.98	0.82
				Average Error		0.77

Error due to instrument during the measurement of wear on the trailing edge of the runner blade was analyzed and calculated and is as shown on the table 3.6 above. And from the calculation, instrument error during measurement of wear at the trailing edge was 0.77%

Table 3.6 shows the error analysis performed during the measurement done on the trailing edge of the blade in all the thirteen number of blades and was found to be 0.77%

CHAPTER FOUR: RESULT AND DISCUSSION

4.1 Sediment Sample test

The sediment of the MMHPS reservoir is taken from the site and is given to the Hydro lab, Krishna Galli for the test. The test performed are of

a) Mineralogical distribution

b) Particle size distribution

The mineral content of the MMHPS reservoir sample are shown in the table 4.1 below.

Table 4.1: Mineralogical distribution of MMHPS Sediment

Minerals		Sample (%)			Average	Hardness (Moh's Scale)
		1	2	3	(%)	
Quartz		57	50	55	54	7
Feldspar		3	3	3	3	6
Mica		9	12	9	10	2-3
Other	A	2	3	4	3	≥5
	B	29	32	29	30	<5

The above table 4.1 shows the content of Quartz, Feldspar, Mica and other minerals i.e. mineralogical classification of MMHPS reservoir and was observed that the content of Quartz is high followed by mica and feldspar.

b) Particle Size Distribution

The particle size distribution of MMHPS reservoir are shown in figure 4.1 and it can be seen from the graph that most of the particles are on the size under range (0.1mm-1mm). Similarly figure 4.2 shows the particle size distribution graph of MMHPS draft tube in which the particles are on the size under range (0.01-0.1) mm. So, in the flow analysis the particle size of 0.1 mm was considered as an input parameter for sand.

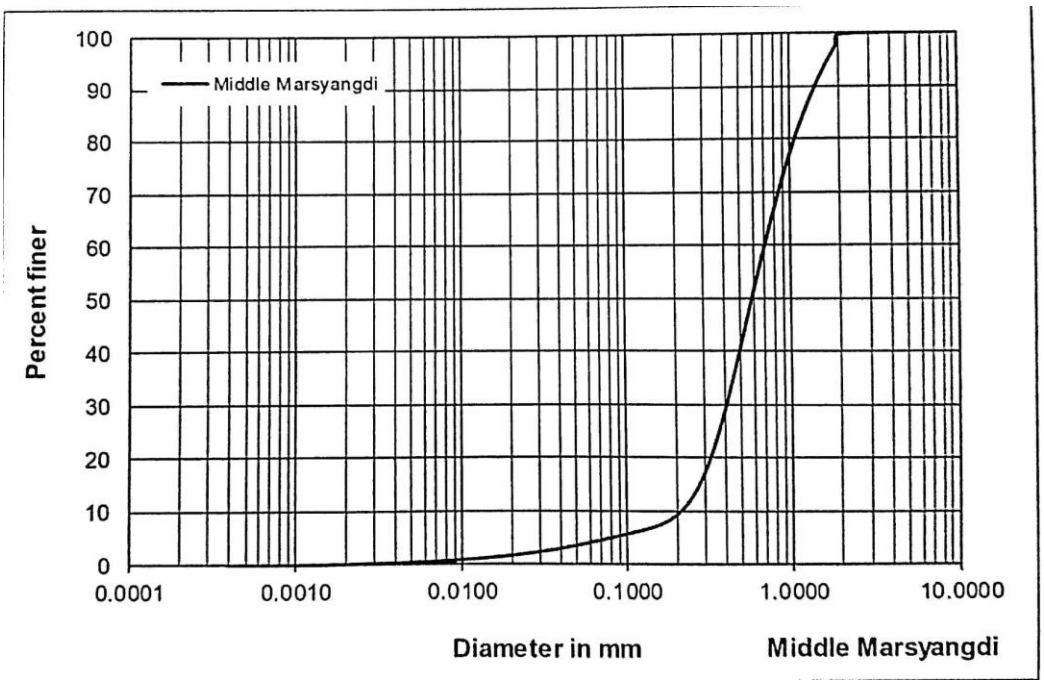

Figure 4.1: Particle size distribution graph of MMHPS reservoir Sediment

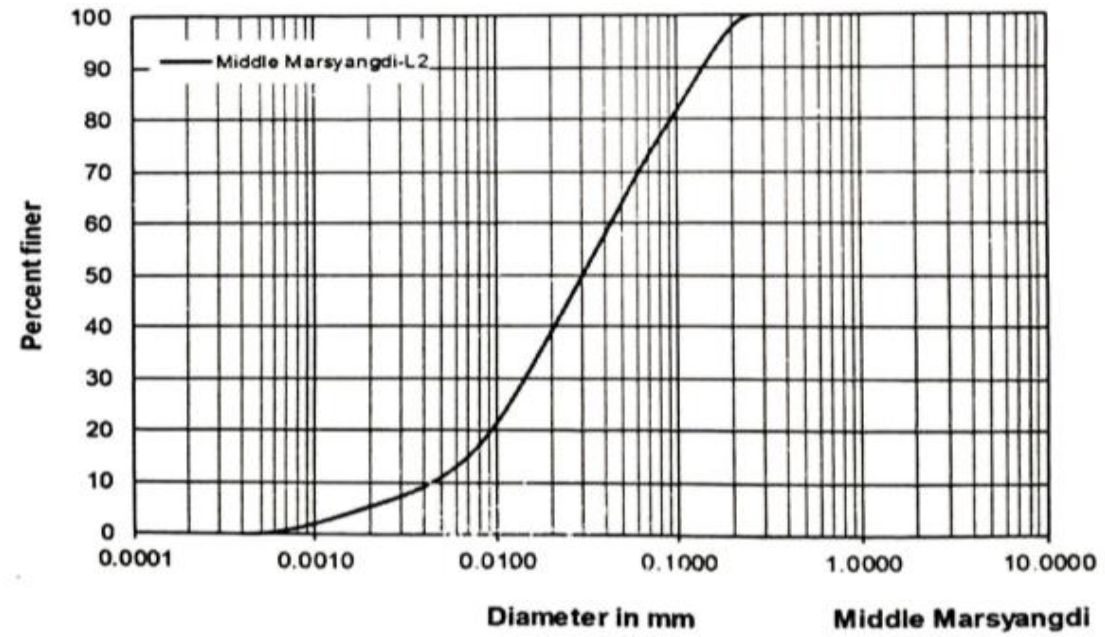

Figure 4.2: Particle size distribution graph of MMHPS draft tube sediment

4.2 Data collections

4.2.1 Sediment Data Collection

All the required data of the year 2018 and 2019 were collected from the site and are shown on figure below. The data available was of the month June, July and august. The

other months are not considered as there consist of lesser amount of sediment compared to these months. Figure 4.3 shows the sediment concentration data of year 2018 and 2019. The vertical axis shows the sediment concentration value and horizontal axis shows the time duration. It shows that the sediment concentration value in the year 2018 was relatively higher than that of 2019 in month July and august. It may be due to the flood occurring in the year 2018 as a result the sediment concentration increased. Sediment concentration is higher in the month July compared to June and august in both the year.

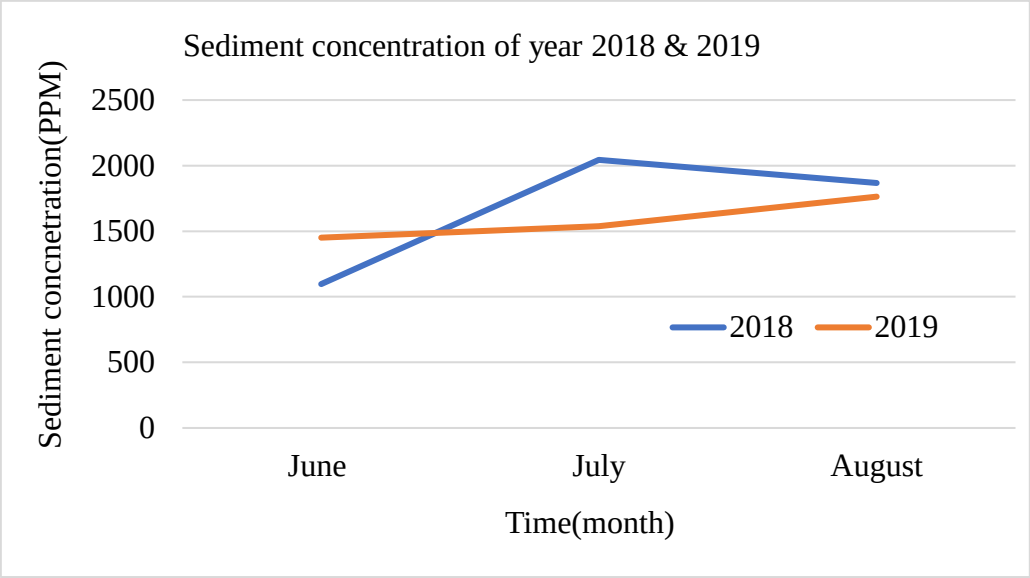

Figure 4.3: Sediment concentration of MMHPS in year 2018 and 2019

4.2.2 Discharge

The discharge data for the peak sediment containing month of June, July and August are shown on the figure 4.4. The vertical axis denotes the discharge values and the horizontal axis shows the time duration. The discharge value of 2019 June was relatively low as it seems that the turbine was operated at part load. In the month of July and august, the discharge value of year 2019 was relatively greater than that of year 2018.The value of discharge was maximum in the month of august for both the year compared to other months.

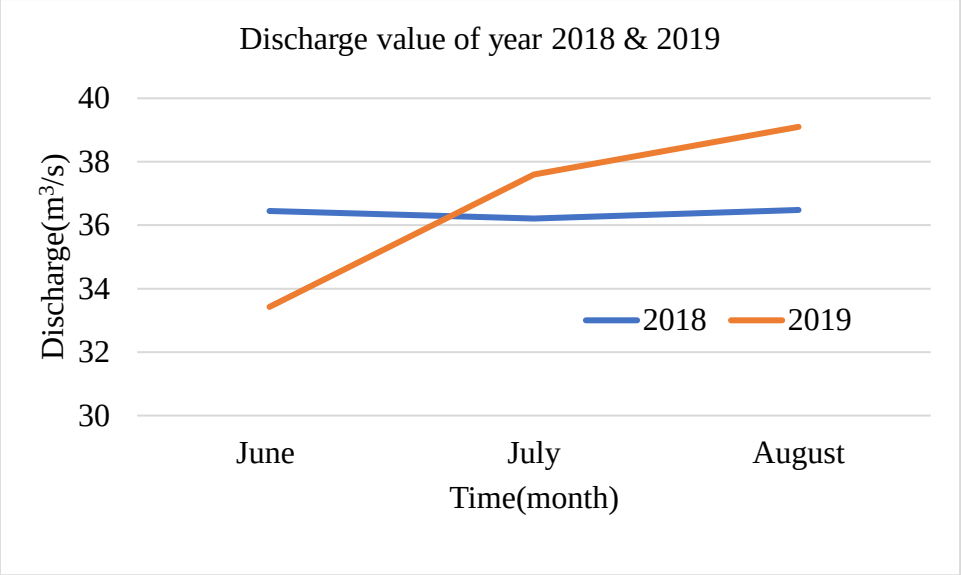

Figure 4.4: Discharge of MMHPS in the year 2018 and 2019

4.2.3 Power generation

The power generated in the year 2018 and 2019 are shown in the figure 4.5. The data was secondary and are collected from the MMHPS control room. The vertical axis shows the power generated in MW and the horizontal values show the month June, July and August. The power generation of June in year 2019 was comparatively lower than that of 2018.It may be due to the low value of discharge or may be due to shutdown of turbine for maintenance. The power generation was maximum in June 2018.

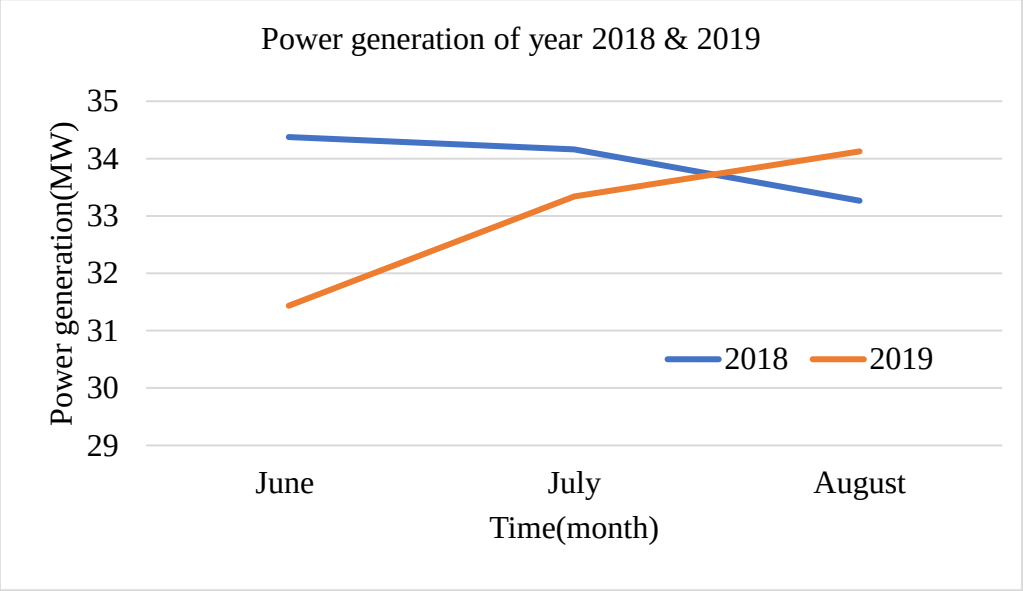

Figure 4.5: Power generation data of MMHPS of year 2018 and 2019

4.3 Results

4.3.1 Simulation Results

The simulation was performed in ANSYS CFX 18.1 using all boundary condition and the erosion pattern was analyzed for three operation condition which are described below.

a. Erosion pattern at full gate opening

Figure 4.6 shows the Erosion rate density of the runner at the pressure and suction side respectively at full gate opening condition. The erosion pattern was obtained and the outlet side of the blade was found to be eroded highly. It may be due to the high velocity sand laden water flowing through trailing edge side of the blade and drop in pressure.

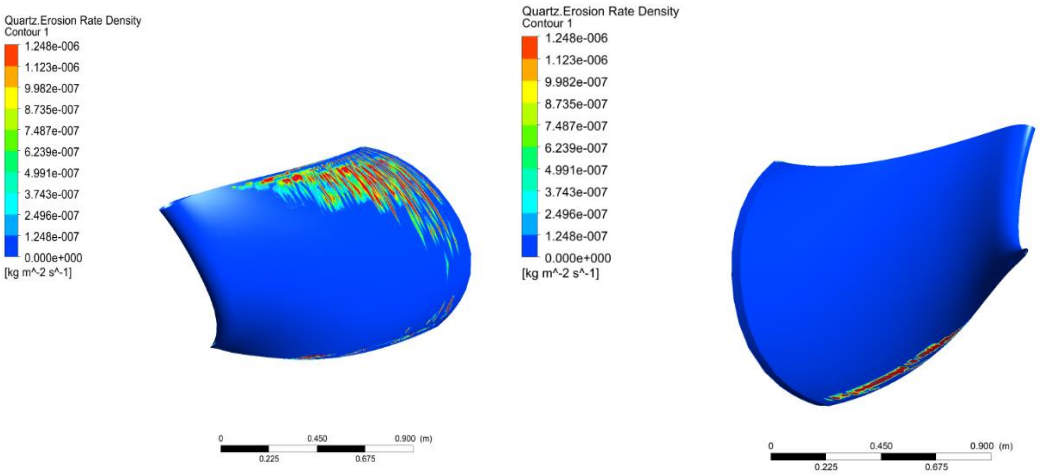

(a) (b)

Figure 4. 6: Erosion pattern in Runner blade on (a) Pressure side (b) Suction side at full load condition

b. Erosion at Best Efficiency point

Figure 4.7 shows the erosion pattern of the runner blade at the best efficiency point with the guide vane opening angle of 24 degrees. The erosion pattern was observed on the trailing edge side. It may due to the curve shaped profile of the blade and high velocity at the outlet. The edge of the blade joining the shroud on the suction side was also eroded. The erosion pattern at the pressure side and the suction side of the blade are as shown below.

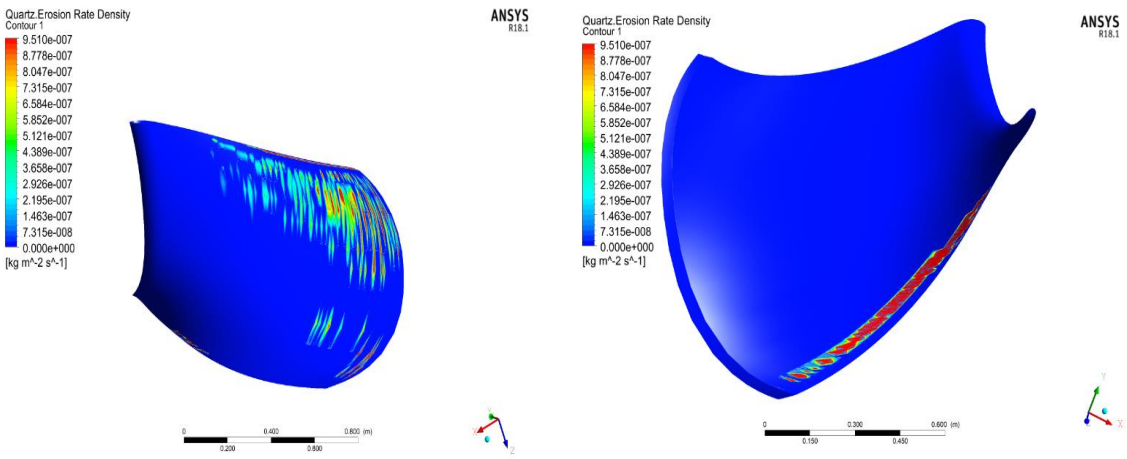

(a) (b)

Figure 4. 7: Erosion pattern of runner blade on (a) Pressure side (b) Suction side at BEP

c. Erosion pattern at Part load condition

The erosion pattern of the runner blade at part load condition at the guide vane opening angle of 16 degrees at the pressure side and the suction side are shown in figure 4.8. The erosion pattern was found on the trailing edge side and was lesser than full load and BEP. It may be due to the lesser amount of flow in part load condition.

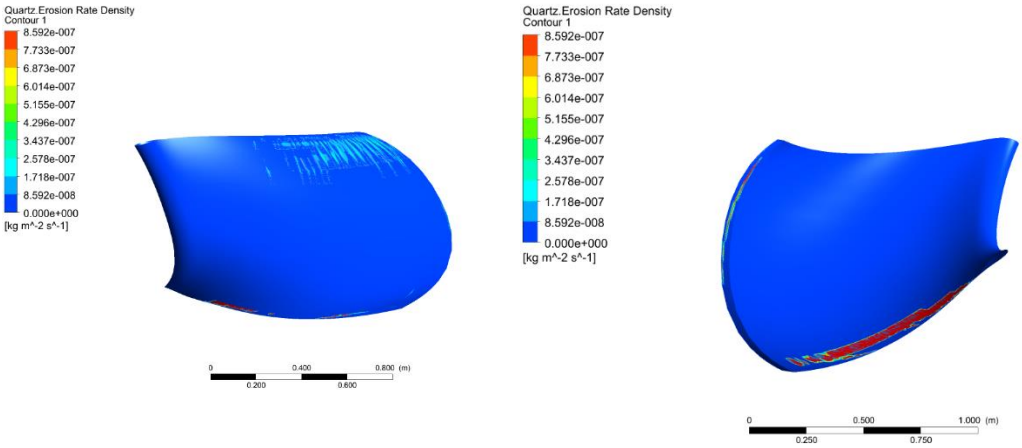

(a) (b)

Figure 4. 8: Erosion pattern of Runner blade at (a) Pressure side (b) Suction side on part load condition

d. Pressure variation at pressure and Suction side

Figure 4.9 shows the pressure distribution of the runner blade and found a smooth transition from the leading to the trailing edge. The distribution on the pressure side was very good, showing a smooth transition. Pressure goes on decreasing moving from leading to trailing edge as shown on the pressure contour. The pressure at the suction side was lesser than that on the pressure side at every point from LE to TE.

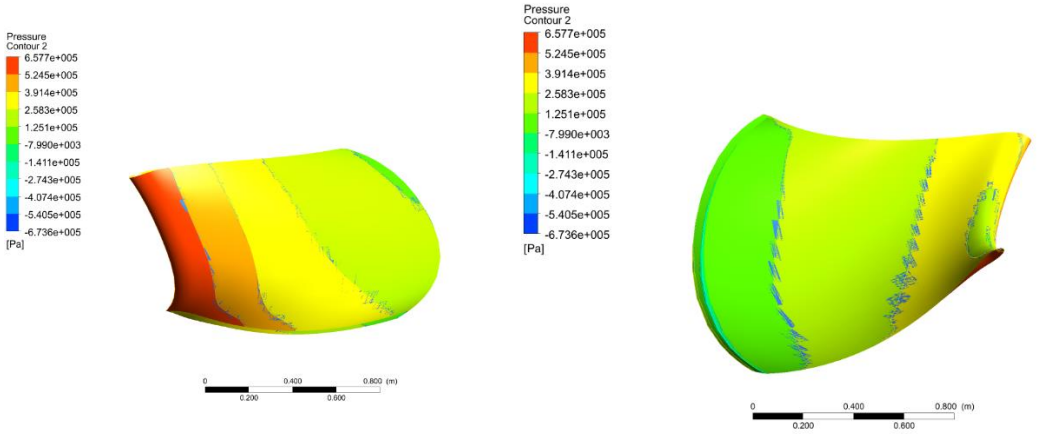

(a) (b)

Figure 4.9: Pressure distribution in runner blade on (a) Pressure side (b) Suction side

e. Velocity distribution

Figure 4.10 shows the variation of velocity from the LE to TE on both the pressure side and the Suction side. The velocity goes on increasing while moving towards the TE from LE on both sides.

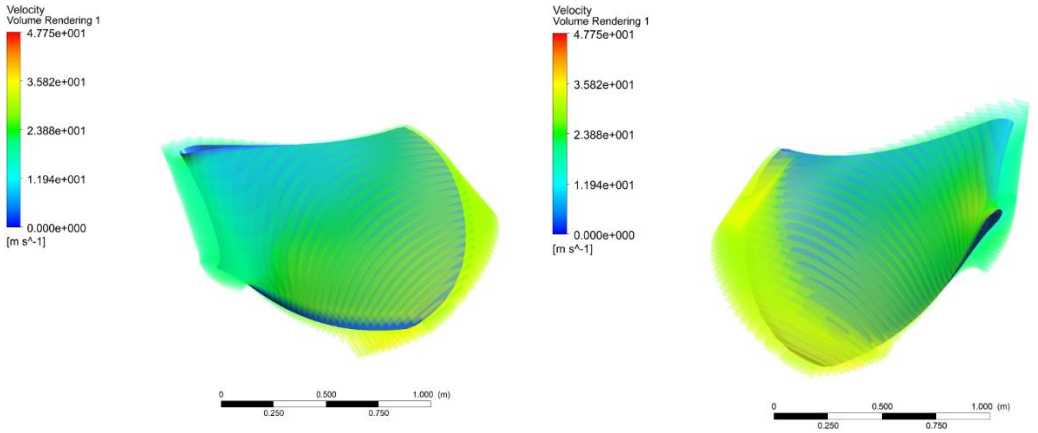

(a) (b)

Figure 4.10: Velocity distribution of Runner blade on (a) pressure side (b) Suction side

f. Erosion Rate density at a different sediment inflow rate

The sediment inflow rate was varied to see the change of erosion rate density. Different flow rate was given at BEP. There was no specific distinction in erosion pattern and the vulnerable region to erosion was almost the same for various inflow rates but erosion rate density increased. The erosion pattern obtained with varying sediment inflow rate are shown on figure 4.11 below.

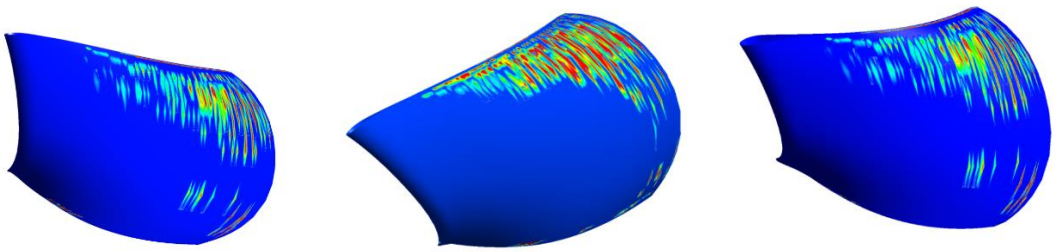

(a) (b) (c)

30 kg/s 40kg/s 50kg/s

Figure 4.11: Erosion pattern at a different mass inflow rate

The variation of Erosion rate density with the sand inflow rate are as shown on figure 4.12. It was clear that with the increase in sand inflow rate, the sediment ERD goes on increasing.

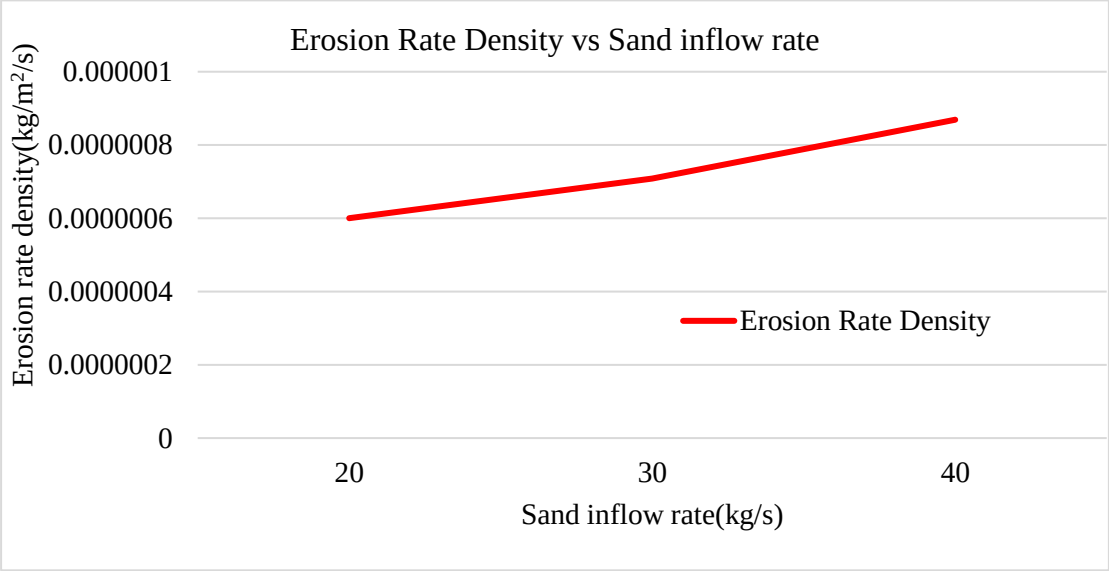

Figure 4.12: Erosion rate density vs Sand inflow rate

g. Erosion rate density at different gate opening

Figure 4.13 shows the variation of erosion rate density with different guide vane opening angles. It was observed that the erosion rate density goes on increasing with the increase in discharge (guide vane opening angle).

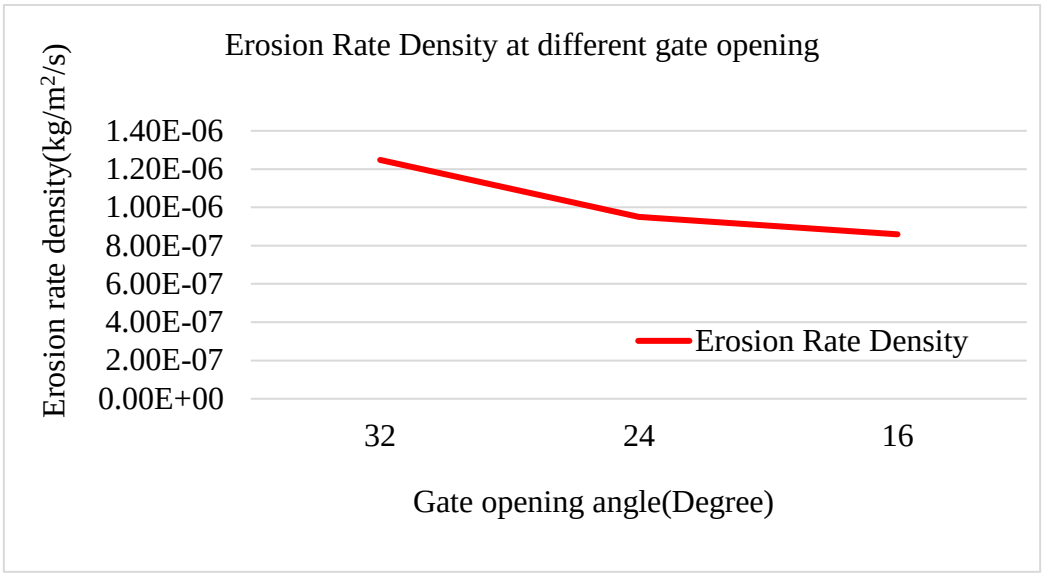

Figure 4.13: Erosion rate density vs Guide vane gate opening

h. Erosion rate density at different Quartz diameter

The erosion rate density was observed by varying the diameter of the Quartz content. The diameter of Quartz was varied from 100 to 200 to 300 micron and erosion rate density was observed. It was noted that with the increase in quartz diameter, the ERD also increases correspondingly.

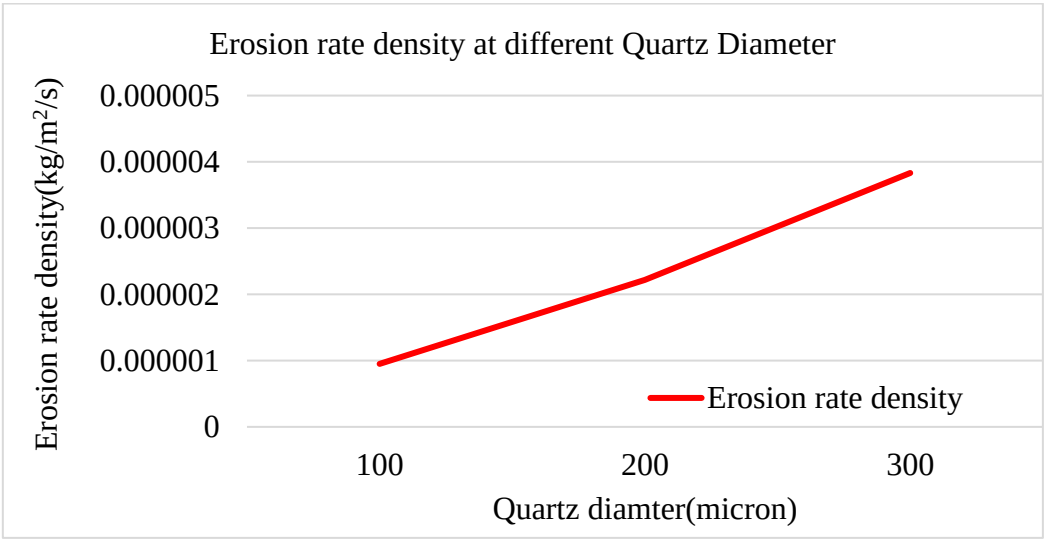

Figure 4. 14: Erosion rate density vs Quartz diameter

4.3.2 Field measurement

The measurement was performed on the site during the overhauling period of 2019. Different tools and techniques were used for the measurement. Transparent paper and pencil were used for tracing the area eroded of blade and results seemed more accurate by this method. The depth of the eroded gap at different places was measured using Vernier caliper with the least count of 0.02mm and average depth was taken from them. On the outlet side, a similar method was performed. The loss of material and coatings area was traced on the paper and assuming different small rectangular sections on paper, the calculation was done to determine the eroded area. The loss of thickness of the blades was calculated by subtracting the originally designed thickness of the runner and the measured thickness during the measurement process.

The erosion portion was divided into two categories:

a. Qualitative analysis

In qualitative analysis, the erosion-prone area was determined by taking the photograph of the dismantled runner during the overhauling period of MMHPS and erosion was most likely to occur on the Inlet side (leading edge) and trailing edge of the blade.

i. Erosion on the inlet (leading edge) side

Due to the direct impact of water with high-velocity water emerging from the guide vane opening, there was the erosion on the inlet (leading) edge of the blade. A larger amount of material loss was found at the inlet portion as shown in figures 4.15.

Figure 4. 15: Erosion pattern in the leading edge of MMHPS runner

ii. Erosion on the outlet of the blade

There was a huge amount of coating loss and reduction in the blade thickness found on the dismantled runner. It was due to the reason that the profile of the runner was curved shaped at the outlet. As a result, there was a direct impulse action of water in the blade as well as water containing sediment flows through high velocity at the outlet and also there was a huge amount of drop in pressure. Consequently, there was the possibility of the problem of cavitation also. The loss of coatings and the materials at the outlet is shown in figure 4.16. It shows there was a loss of coatings and materials of runner blade and tears detected in the outlet of the runner blade.

Figure 4. 16: Erosion pattern and tear in the trailing edge

b. Quantitative analysis

From the eroded area, it was multiplied with the depth of erosion to determine the volume. Now multiplying the eroded volume by the density of turbine material (ρ=7800kg/m^3) eroded mass was calculated. A large amount of void gap (material loss) was seen in some of the blades in the inlet and similar types of mass erosion were seen on all the thirteen blades. All these eroded masses were calculated from all thirteen number of blades and the results are shown below.

i. Mass eroded in the leading edge (inlet part) in all blades

The eroded mass in the leading edge was calculated using the measuring scale and Vernier caliper. Uniform type of erosion was seen in all the thirteen number of blades with local large wear in some blades and the total eroded mass in the leading edge in all the blades is shown on the table 4.2 below.

Table 4.2: Eroded mass in the Leading edge

Blade no	Uniform type of erosion(gm)	Local large wear(gm)	Total eroded mass(gm)
1	120	0	120
2	120	40	160
3	120	0	120
4	120	0	120
5	120	20	140
6	120	0	120
7	120	0	120
8	120	70	190
9	120	0	120
10	120	0	120
11	120	0	120
12	120	0	120
13	120	40	160
Total	1560	170	1730

ii. Mass eroded and loss in thickness at the outlet of the blade

The uniform erosion in all the thirteen blades was calculated. The height and breadth were calculated by tracing the eroded surface in paper and thickness are measured by using Vernier caliper. Now the loss in thickness(depth) was calculated by subtracting the original thickness and the measured thickness. The average loss of material from each blade was found to be 1630.79 gm.

Table 4.3: Eroded mass calculation in the trailing edge (outlet) of the blade

	Uniform Erosion on Outlet of Blades						
BN	Height (mm)	Base (mm)	Area (mm^2)	Depth (mm)	Worn Volume (mm^3)	Worn Mass(gm)	Total Worn Mass (gm)
1	550	210	57750	3.3	190.58	1486.49	
2	430	380	81700	4.5	367.65	2867.67	
3	600	350	105000	3.35	351.75	2743.65	
4	230	440	50600	3.45	174.57	1361.65	
5	350	230	40250	5.6	225.40	1758.12	
6	390	280	54600	3.5	191.10	1490.58	
7	530	150	39750	4.5	178.88	1395.23	21200.31
8	230	300	34500	2.1	72.45	565.11	
9	480	195	46800	2.4	112.32	876.10	
10	600	332	99600	3.8	378.48	2952.14	
11	320	176	28160	4.9	137.98	1076.28	
12	290	430	62350	3.1	193.29	1507.62	
13	330	300	49500	2.9	143.55	1119.69	
				Average loss in one blade			1630.7934

iii. Total eroded mass

The total eroded mass on each blade is the sum of eroded mass in the leading edge and eroded mass in trailing edge as shown below in table 4.4.

Table 4.4: Total eroded mass in thirteen blades

Blade no	Eroded mass in the leading edge(gm)	Eroded mass in the outlet of the blade(gm)	Total eroded mass in each blade(gm)
1	120	1490	1610
2	160	2870	3030
3	120	2740	2860
4	120	1360	1480
5	120	1760	1880
6	120	1490	1610
7	120	1400	1520
8	190	570	760
9	120	880	1000
10	120	2950	3070
11	120	1080	1200
12	120	1510	1630
13	160	1120	1280
Average	1710	21220	22930

iv. Loss in thickness at trailing edge

The thickness was measured using Vernier caliper and by subtracting the obtained thickness from the original thickness of the blade, the loss in thickness was obtained. The loss of thickness obtained from all the thirteen number of blades and the average loss of thickness of the blade of MMHPS was found 3.646 mm every two years of operation as shown in table 4.5.

Table 4.5: Loss in thickness of runner blade at the outlet

Blade no	Observed thickness(mm)	loss in thickness(mm)
1	6.7	3.3
2	5.5	4.5
3	6.65	3.35
4	6.55	3.45
5	4.4	5.6
6	6.5	3.5
7	5.5	4.5
8	7.9	2.1
9	7.6	2.4
10	6.2	3.8
11	5.1	4.9
12	6.9	3.1
13	7.1	2.9
Average	6.35	3.65

c. Qualitative results comparison

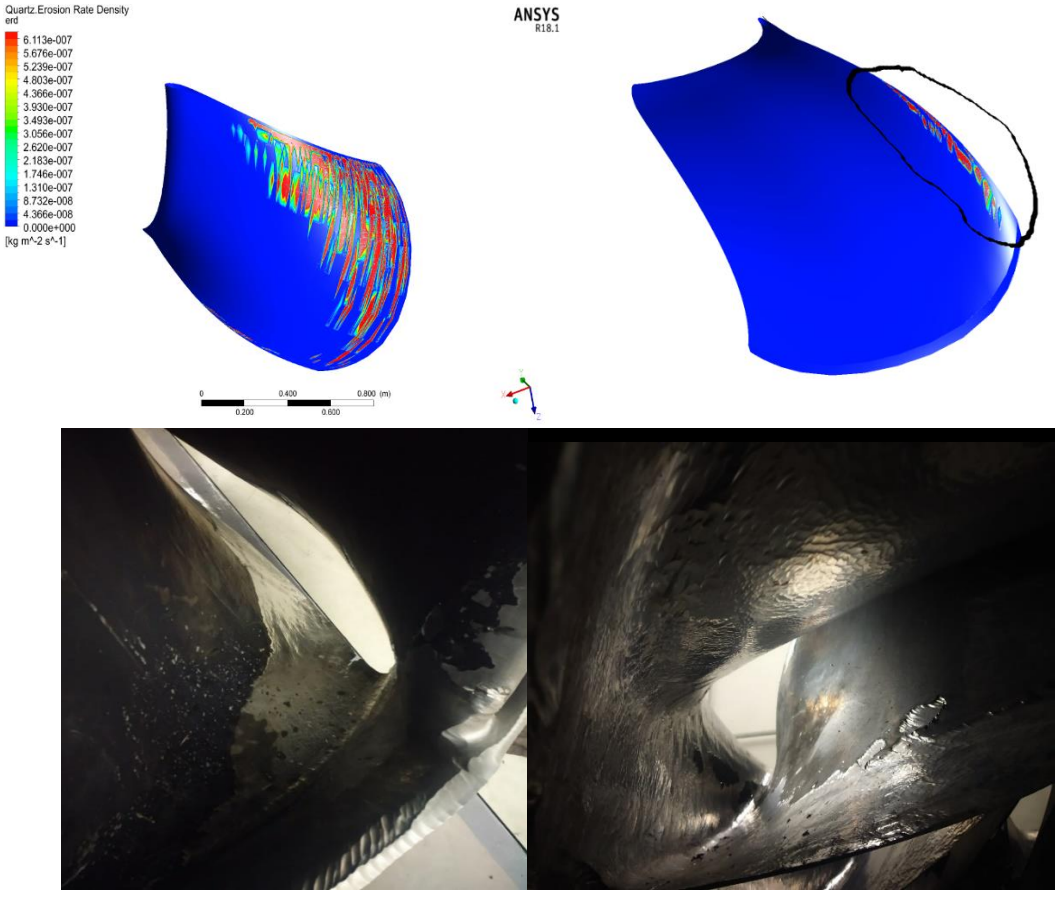

Figure 4.17: Comparison of Erosion pattern at the outlet of the runner

The qualitative result was obtained and the erosion pattern was observed. The qualitative result from the field visit was obtained through a photograph taken from the dismantled runner from the site during the overhauling period of 2019. The qualitative result for numerical analysis was obtained through the flow simulation. The qualitative result obtained from both the site visit and simulation analysis was found to be of similar type and is shown in above figure 4.17.

d. Erosion rate density comparison

The measurement of wear and amount of mass removed was measured from the site. The eroded surface was traced in the paper and the depth of erosion and thickness loss were measured using Vernier caliper. Now by multiplying the eroded mass by the area of the blade and operational time we get erosion rate density.

Table 4.6: Comparison of ERD at full load condition

Blade no	Erosion Rate density from site visit($kg/m^2/s$)	Erosion Rate density From Simulation($kg/m^2/s$)	Difference in Erosion rate density($kg/m^2/s$)	% Difference
1	5.63307E-08	1.25E-06	1.19167E-06	95.49
2	2.81654E-07	1.25E-06	9.66346E-07	77.43
3	6.75969E-07	1.25E-06	5.72031E-07	45.84
4	2.25323E-07	1.25E-06	1.02268E-06	81.95
5	1.12661E-07	1.25E-06	1.13534E-06	90.97
6	3.37984E-07	1.25E-06	9.10016E-07	72.92
7	5.63307E-07	1.25E-06	6.84693E-07	54.86
8	4.50646E-07	1.25E-06	7.97354E-07	63.89
9	5.06977E-07	1.25E-06	7.41023E-07	59.38
10	3.94315E-07	1.25E-06	8.53685E-07	68.40
11	6.19638E-07	1.25E-06	6.28362E-07	50.35
12	1.68992E-07	1.25E-06	1.07901E-06	86.46
13	7.32300E-07	1.25E-06	5.157E-07	41.32
Average	3.94315E-07	1.25E-06	8.53685E-07	68.40

Now the Erosion rate density so obtained from the field visit was compared with the erosion rate density obtained from the Simulation analysis. The erosion rate density obtained from the site measurement was comparatively lower than that of simulation for all the three operating conditions and it may be due to Elastomeric semi-soft coatings used in the runner blade on site. The ERD results from both the analysis at full load condition are shown on the table.4.6 above. Percentage difference in ERD was found to be 68%. and the Metaline Elastomeric Semi soft coating used in MMHPS runner blade seem to be effective.

Table 4.7: Comparison of ERD at Best efficiency point (BEP)

Blade no	Erosion Rate density from site visit($kg/m^2/s$)	Erosion Rate density From Simulation($kg/m^2/s$)	Difference in Erosion rate density($kg/m^2/s$)	% Difference
1	5.63307E-08	9.51E-07	8.94669E-07	94.08
2	2.81654E-07	9.51E-07	6.69346E-07	70.38
3	6.75969E-07	9.51E-07	2.75031E-07	28.92
4	2.25323E-07	9.51E-07	7.25677E-07	76.31
5	1.12661E-07	9.51E-07	8.38339E-07	88.15
6	3.37984E-07	9.51E-07	6.13016E-07	64.46
7	5.63307E-07	9.51E-07	3.87693E-07	40.77
8	4.50646E-07	9.51E-07	5.00354E-07	52.61
9	5.06977E-07	9.51E-07	4.44023E-07	46.69
10	3.94315E-07	9.51E-07	5.56685E-07	58.54
11	6.19638E-07	9.51E-07	3.31362E-07	34.84
12	1.68992E-07	9.51E-07	7.82008E-07	82.23
13	7.32300E-07	9.51E-07	2.187E-07	23.00

The erosion rate density was obtained from both the analysis as shown in the above table 4.7. It was found that the deviation in ERD at BEP was 58 % in average. The erosion rate obtained at BEP was compared to be lesser than obtained at full load condition. So, it is beneficial to operate the turbine at BEP rather than at full load at peak sediment containing month for better operation.

Table 4.8: Comparison of ERD at Part load condition

Blade no	Erosion Rate density from site visit($kg/m^2/s$)	Erosion Rate density From Simulation($kg/m^2/s$)	Difference in Erosion rate density($kg/m^2/s$)	% Difference
1	5.63307E-08	8.592E-07	8.02869E-07	93.44
2	2.81654E-07	8.592E-07	5.77546E-07	67.22
3	6.75969E-07	8.592E-07	1.83231E-07	21.33
4	2.25323E-07	8.592E-07	6.33877E-07	73.78
5	1.12661E-07	8.592E-07	7.46539E-07	86.89
6	3.37984E-07	8.592E-07	5.21216E-07	60.66
7	5.63307E-07	8.592E-07	2.95893E-07	34.44
8	4.50646E-07	8.592E-07	4.08554E-07	47.55
9	5.06977E-07	8.592E-07	3.52223E-07	40.99
10	3.94315E-07	8.592E-07	4.64885E-07	54.11
11	6.19638E-07	8.592E-07	2.39562E-07	27.88
12	1.68992E-07	8.592E-07	6.90208E-07	80.33
13	7.32300E-07	8.592E-07	1.269E-07	14.77
Average	3.94315E-07	8.592E-07	4.64885E-07	54.11

The erosion rate density was obtained from both Field measurement and Simulation analysis as shown in the above table 4.8. It was found that the difference in result obtained was 54.11%. The difference so obtained was lesser than the difference obtained at full load condition and BEP.As the load on the runner go on decreased, the difference obtained also decreased. The difference so obtained in the result was may be due to the use of Elastomeric semi-soft coatings used in MMHPS runner blades.

CHAPTER FIVE: CONCLUSIONS AND RECOMMENDATIONS

5.1 Conclusions

The major findings of this thesis work have been summarized as follows.

- Erosion was observed to be maximum on the trailing edge of MMHPS runner. The eroded mass of all the runner blades in total was found to be 22.93 kg while the average thickness loss at the trailing edge was 3.65 mm per blade. The average erosion rate density at full load condition was determined to be 3.94E-07 $kg/m^2/sec$.
- The erosion pattern on the blades were observed to be maximum on the trailing edges which resembles the site conditions of runner. However, the ERD at full load was relatively higher (1.28E-6 $kg/m^2/sec$) than those obtained at BEP (9.51E-7 $kg/m^2/sec$) and part load condition (8.59E-7 $kg/m^2/sec$). This suggests that it is suitable to operate the runner at BEP during peak sediment months (June, July and August). Also, this study enables us to predict the erosion pattern and erosion rate density if the corresponding sediment data are available.
- The deviation on average erosion rate density at full load condition between site measurement and numerical analysis was found to be 68%.
- The Elastomeric semi soft coating used in MMHPS runner seems to be fruitful.

5.2 Recommendations

The following recommendations can be suggested for further study

- 3D scanning of runner can be done to achieve more precise runner design.
- Flow analysis of the runner as whole could give deep insight on the overall erosion pattern and erosion rate density.
- Use of coatings during runner modeling can be done to resemble the actual site conditions thereby providing us with more accurate results.

REFERENCES

ANSYS. (2006). CFX Solver theory guide. 1996--2006. Cannonsburg: ANSYS Inc. Retrieved June 23, 2020, from https://www.academia.edu/6123972/ANSYS_CFX-Solver_Theory_Guide_ANSYS_CFX_Release_11.0

ANSYS. (2011). CFX Introduction. Cannonsburg: ANSYS Inc. Retrieved June 22, 2020, from http://read.pudn.com/downloads500/ebook/2077964/cfx_intr.pdf

Bergmann-Paulsen, J. (2012). FSI-analysis of a Francis turbine. *Institutt for energi-og prosessteknikk*. DOI:10.5293/IJFMS.2014.7.3.101

Bishwakarma, M., & St{\o}le, H. (2008). Real-time sediment monitoring in hydropower plants. *Journal of Hydraulic Research, 46*, 282--288. DOI:10.1080/00221686.2008.9521862

Coello, C. A., & Zacatenco, C. S. (2012). List of references on constraint-handling techniques used with evolutionary algorithms. *Information Sciences*, 146--168. DOI:10.1145/1830761.1830910

Gautam, S. (2019). Sediment erosion in low specific speed francis turbines: A case study on effects and causes. *Sciencedirect*, 16. DOI:10.1016/j.wear.2019.203152

Kang, M.-W., Park, N., & Suh, S.-H. (2016). Numerical study on sediment erosion of Francis turbine with different operating conditions and sediment inflow rates. *Procedia Eng, 157*, 457--464. DOI:10.1016/j.proeng.2016.08.389

Khanal, K., Neopane, H. P., Rai, S., Thapa, M., Bhatt, S., & Shrestha, R. (2016). A methodology for designing Francis runner blade to find minimum sediment erosion using CFD. *Renewable energy*, 307--316.

Koirala, R., Thapa, B., Neopane, H. P., Zhu, B., & Chhetry, B. (2016). Sediment erosion in guide vanes of Francis turbine: A case study of Kaligandaki Hydropower Plant, Nepal. *Wear*, 53--60. DOI:10.1016/j.wear.2016.05.013

Masoodi, J. H., & Harmain, G. (2017). A methodology for assessment of erosive wear on a Francis turbine runner. *Energy, 118*, 644--657. DOI:10.1016/j.energy.2016.10.095

Masoodi, J., & Harmain, G. (2017). Sediment erosion of Francis turbine runners in the Himalayan region of India. *The International Journal on Hydropower \& Dams*, 82--89. DOI:10.1016/j.wear.2017.02.040

MetaLine. (n.d.). *MetaLine wear protection*. Retrieved August 21, 2020, from https://metaline.com/en/products/series-700-elastomers-sprayable/metaline-785-semi-soft.html

NEA. (2020). *Nepal Electricity Authority*. Retrieved June 20, 2020, from https://www.nea.org.np/genDirectorate

Neopane, H. P. (2010). ediment erosion in hydro turbines and its effect on the flow around guide vanes of Francis turbine. *Tapir Uttrykk*. DOI:10.1016/j.rser.2015.04.178

Noon, A. A. (2017). Erosion wear on Francis turbine components due to sediment flow. *Wear, 378*, 126--135. DOI:10.1016/j.wear.2017.02.040

Padhy, M. K., & Saini, R. (2008). A review on silt erosion in hydro turbines. *Renewable and Sustainable Energy Reviews, 12*, 1974--1987. DOI:10.1016/j.rser.2007.01.025

Padhy, M., & Saini, R. (2012). Study of silt erosion mechanism in Pelton turbine buckets. *Energy, 39*, 286--293. DOI:10.1016/j.energy.2012.01.015

Pandit, H. P., & shakya, H. (2018). Sediment handling in Himalayan rivers using hydrocyclones. *ISH Journal of Hydraulic Engineering*. DOI:10.1080/09715010.2008.10514909

Poudel, L. (2016). Study on sediment characterization and its impact on hydraulic turbine material. DOI:10.3126/njst.v13i2.7725

Pradhan, P. M. (2004). Improving sediment handling in the Himalayas. *OSH research, Nepal*, 1--6. DOI:10.13140/RG.2.2.19074.58561

Rakibuzzaman, M., Kim, H.-H., Kim, K., Suh, S.-H., & Kim, K. Y. (2019). Numerical Study of Sediment Erosion Analysis in Francis Turbine. *Sustainability, 11*, 1423. DOI:10.3390/su11051423

Regmi, N., Dura, H., & Shakya, S. R. (2019). Design and Analysis of Gravitational Water Vortex Basin and Runner. *Proceedings of IOE Graduate Conference*.

Schleiss, A. J., Franca, M. J., Juez, C., & De Cesare, G. (2016). Reservoir sedimentation. *Journal of Hydraulic Research, 54*, 595--614. DOI:10.1080/00221686.2016.1225320

Shrestha, K. P., Thapa, B., Dahlhaug, O. G., Neupane, H. P., Gurung, N., & Kayastha, A. R. (2013). Optimized design of francis turbine runner for sand laden water. *Hydro Nepal: Journal of Water, Energy and Environment, 13*, 36--43. DOI:10.3126/hn.v13i0.10038

Singh, M., Banerjee, J., Patel, P., & Tiwari, H. (2013). Effect of silt erosion on Francis turbine: a case study of Maneri Bhali Stage-II, Uttarakhand, India. *ISH Journal of Hydraulic engineering*, 1--10. DOI:10.1080/09715010.2012.738507

Stachowiak, G. W., & Batchelor, A. W. (2001). Abrasive, erosive and cavitation wear. *Engineering tribology*, *12*. DOI:10.1016/S0167-8922(08)70585

Thapa, B. S., Dahlhaug, O. G., & Thapa, B. (2015). Sediment erosion in hydro turbines and its effect on the flow around guide vanes of Francis turbine. *Renewable and Sustainable Energy Reviews, 49*, 1100--1113. DOI:10.1016/j.renene.2017.01.045

Thapa, B. S., Thapa, B., & Dahlhaug, O. G. (2012). Current research in hydraulic turbines for handling sediments. *Energy*, *47*, 62--69. DOI:10.1080/14634980500218241

Thapa, B. S., Thapa, B., & Dahlhaug, O. G. (2012). Empirical modelling of sediment erosion in Francis turbines. *Energy, 41*, 386--391. DOI:10.1016/j.energy.2012.02.066

Thapa, B., Shrestha, R., Dhakal, P., & Thapa, B. S. (2005). Problems of Nepalese hydropower projects due to suspended sediments. *Aquatic Ecosystem Health \& Management, 8*, 251--257. DOI:10.1080/14634980500218241

PUBLICATION

Devkota, P. R., Poudel, L., Poudyal, A., Regmi, N., & Dahal, D. R. (2020). *Sand Erosion in Francis Runner: A Case study of Middle Marsyangdi Hydropower Station.* IOE Graduate Conference. Kathmandu.

APPENDIX A: RUNNER PICTURES

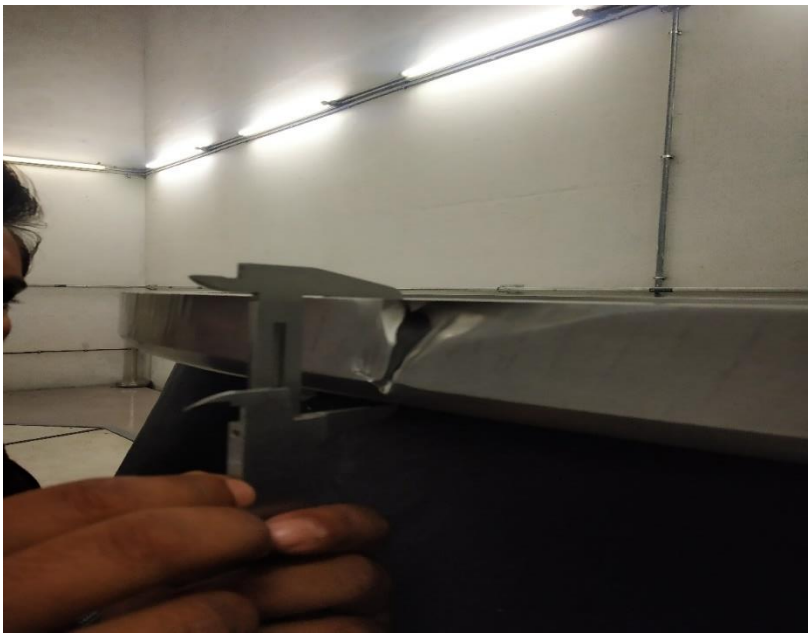

Figure A.1: Measurement of erosion outside Crown of runner

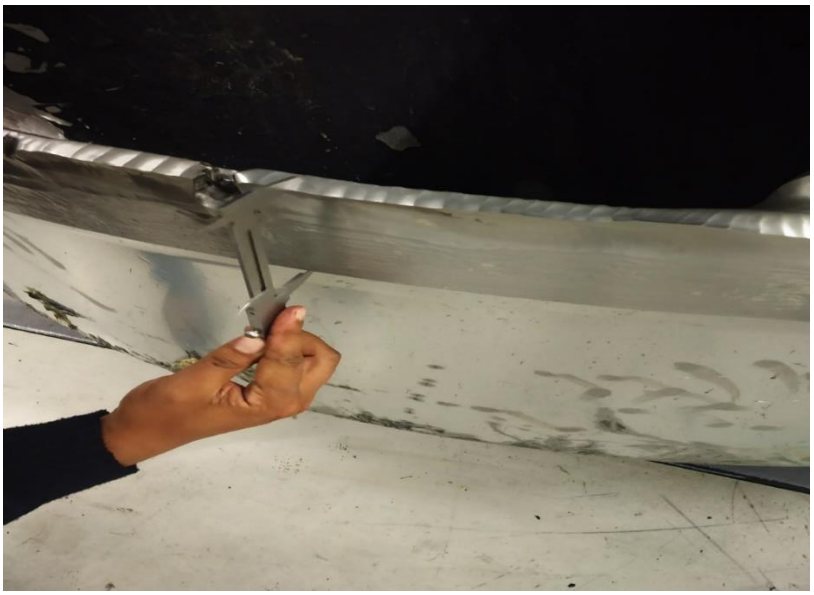

Figure A.2: Measurement of erosion depth
using Vernier caliper outside Band

Figure A.3: Erosion detected outside band

Figure A.4: Erosion detected in the leading edge and band side

Figure A.5: Erosion detected in joining of shroud and blade (inlet side of Shroud)

Figure A.6: Tear detected in the outlet side of runner blade

Figure A.7: Design of MMHPS runner profile in Bladegen

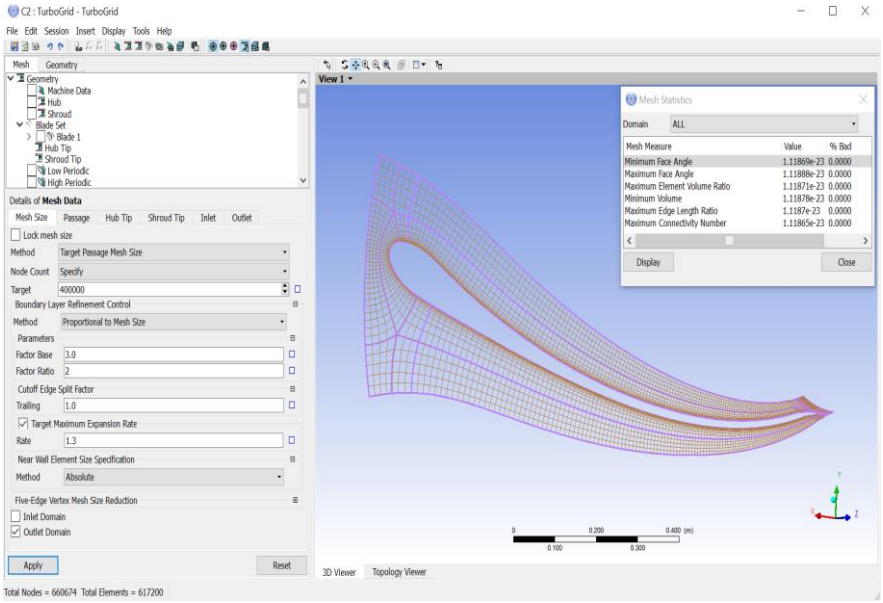

Figure A.8: Setting up parameters required for meshing

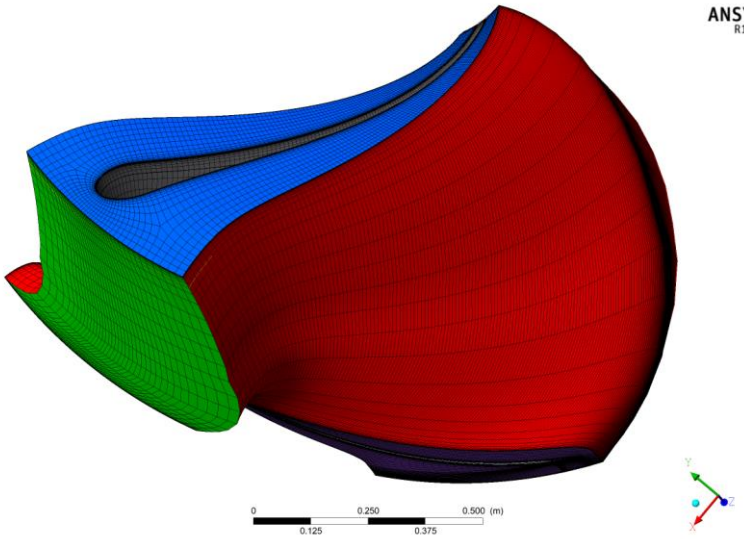

Figure A.9: Meshing on Blade domain

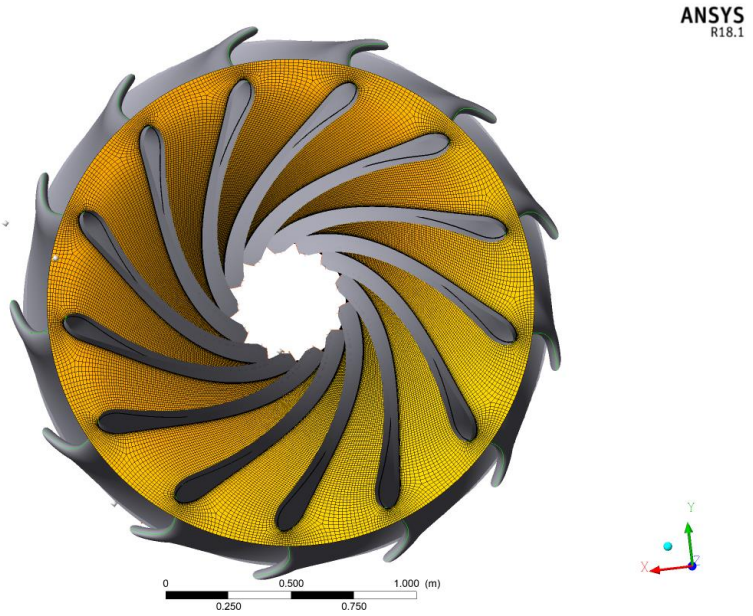

Fig A.10: Mesh generation in all blade domain

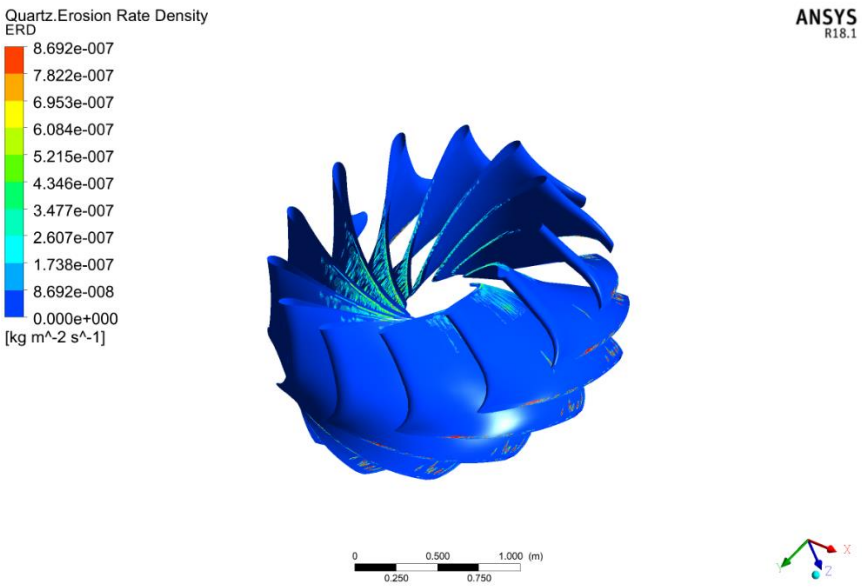

Figure A.10: Quartz erosion rate density in Runner blade

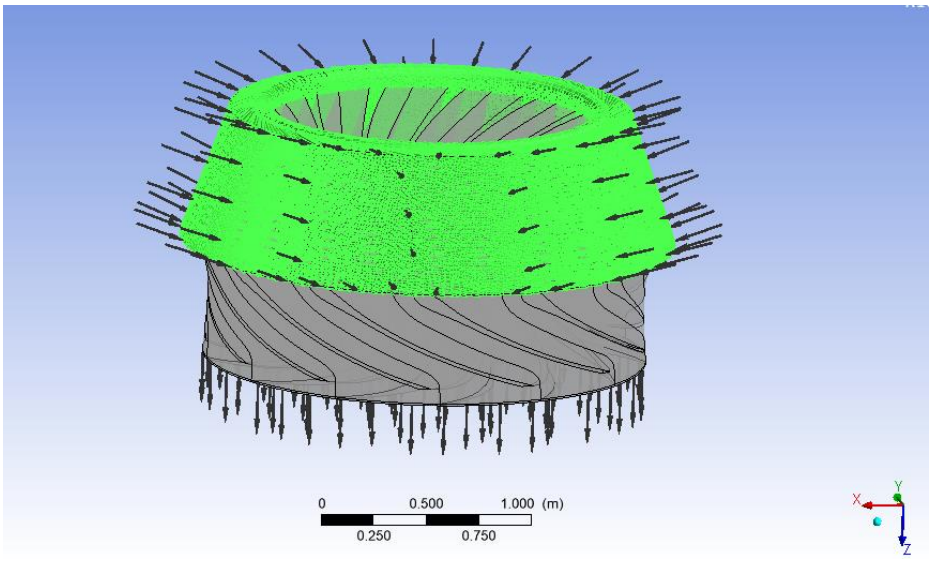

Figure A.12: Fluid domain of inlet of Runner

APPENDIX B: BLADEGEN FIGURES

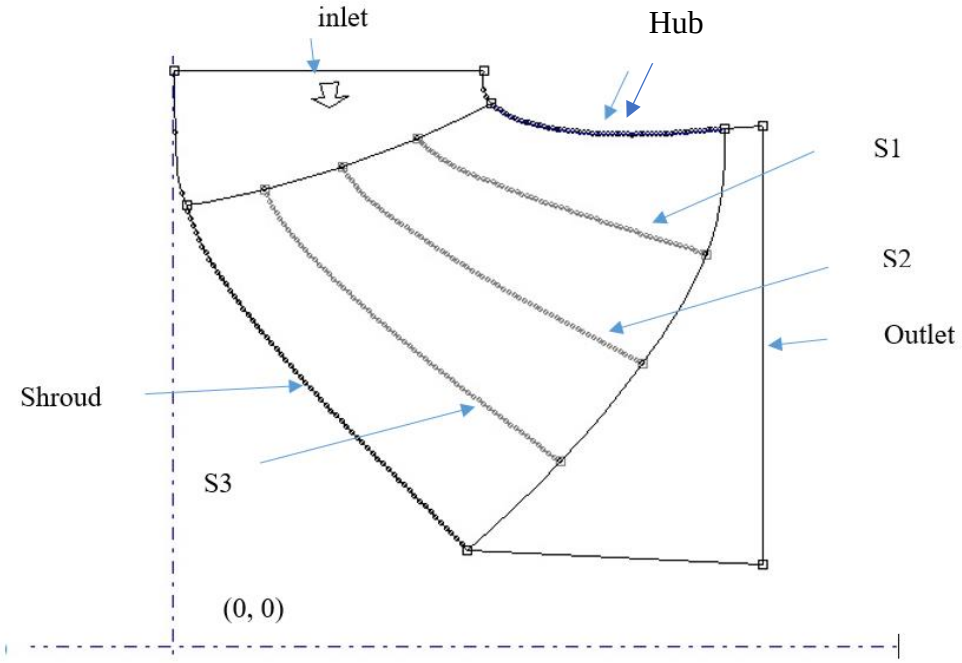

Figure B.1: Meridional view of MMHPS runner in Bladegen

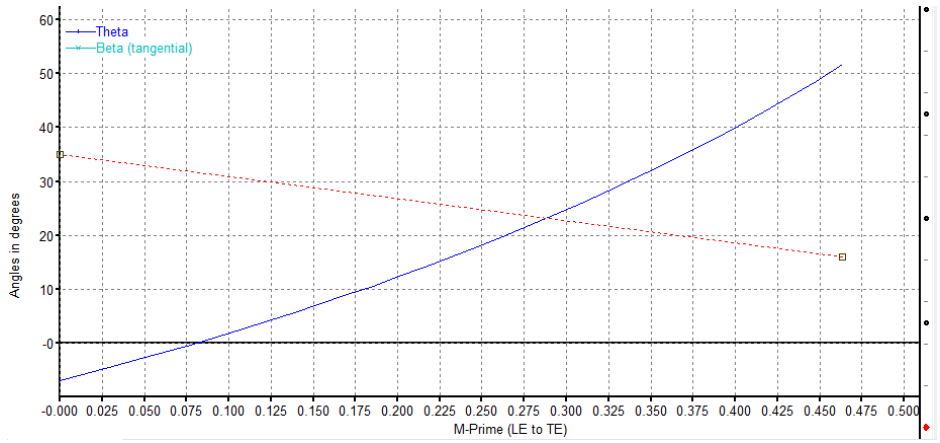

Figure B.2: β-angle distribution graph in BladeGen

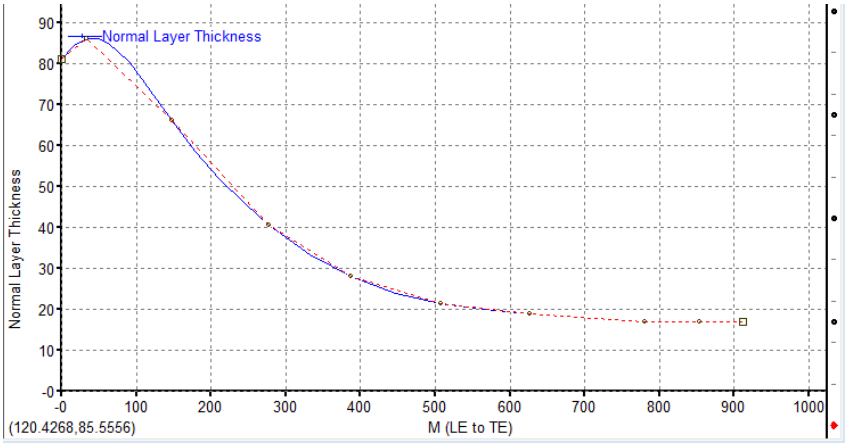

Figure B.3: Blade thickness curve in BladeGen

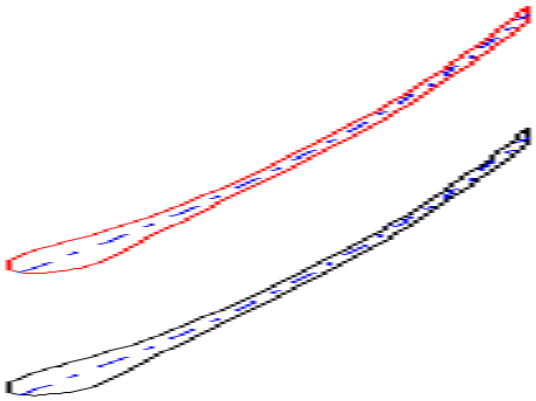

Figure B.4: Blade to blade view in BladeGen

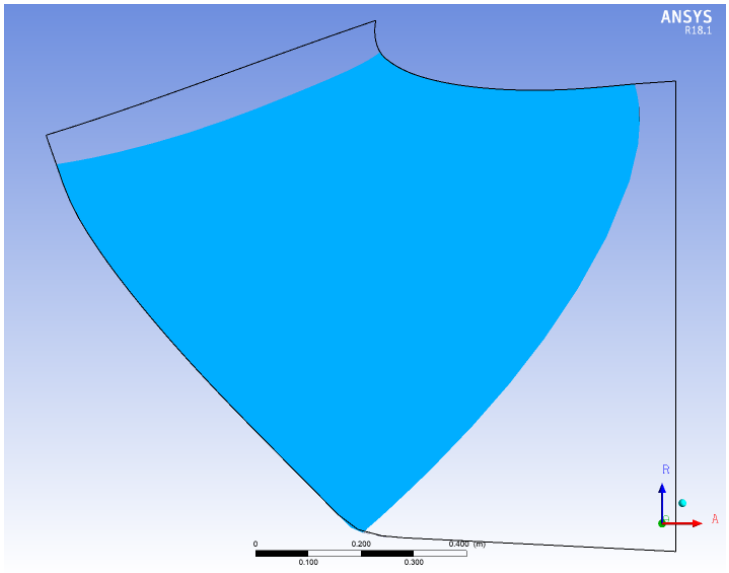

Figure B5: Meridional view of Blade, hub and shroud

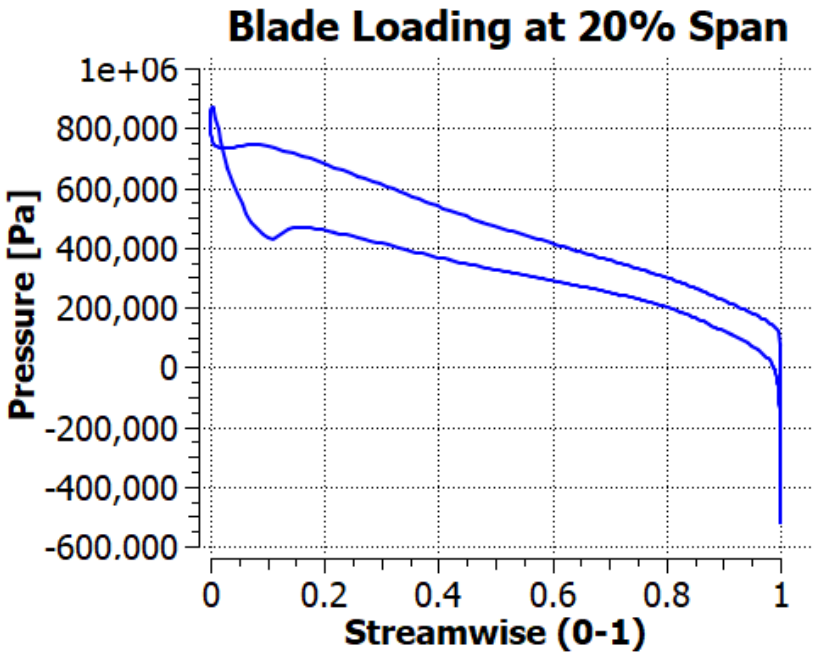

Figure B6: Blade loading at 20% span

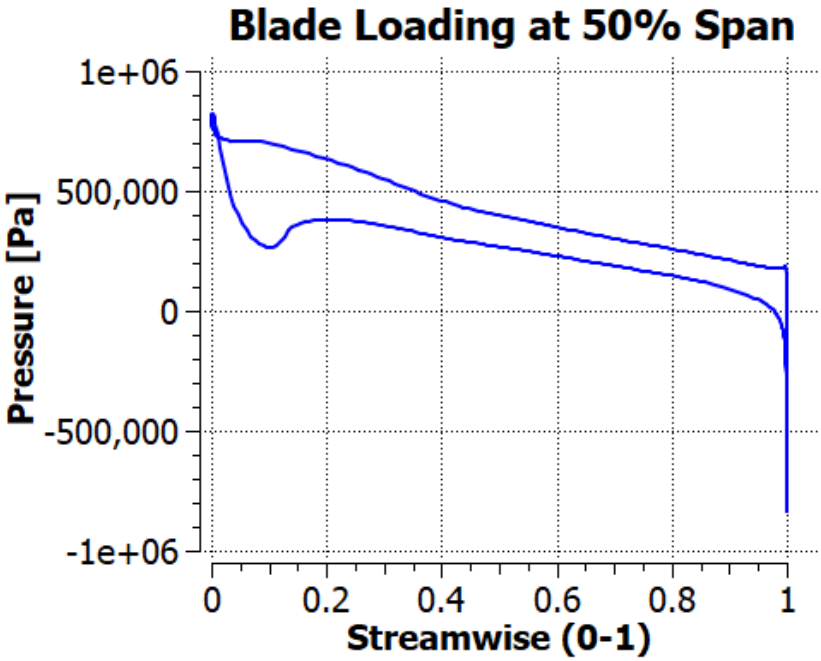

Figure B7: Blade loading at 50% span

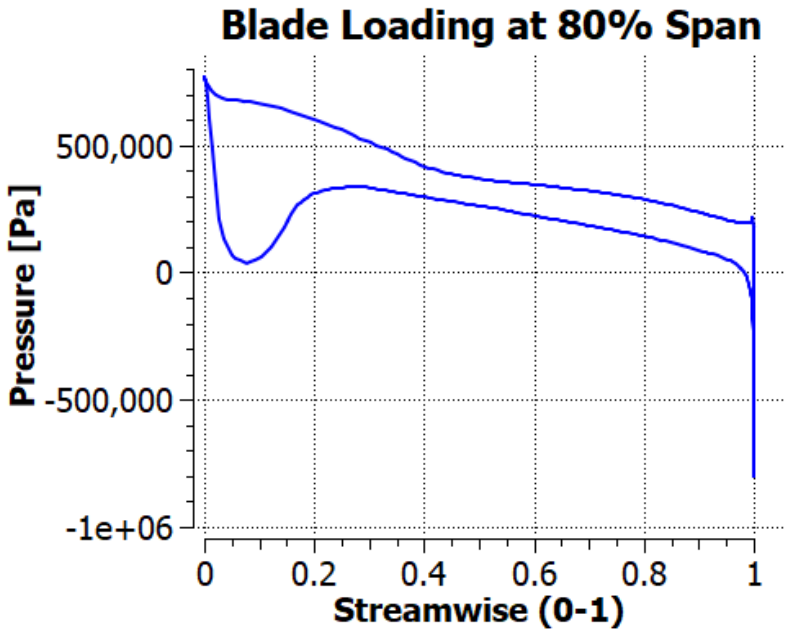

Figure B8: Bade loading at 80% span

APPENDIX C: TABLES USED IN RESULT CALCULATION

Gate opening	Erosion Rate Density(kg/m^2/s)
32	1.25E-06
24	9.51E-07
16	8.59E-07

Sediment inflow rate(kg/s)	Erosion rate density(kg/m^2/s)
30	7.13241E-07
40	9.51E-07
50	1.8873E-06

Quartz diameter(micron)	Erosion rate density(kg/m^2/s)
100	0.000000951
200	2.21695E-06
300	3.8314E-06

APPENDIX D: ORIGINALITY REPORT

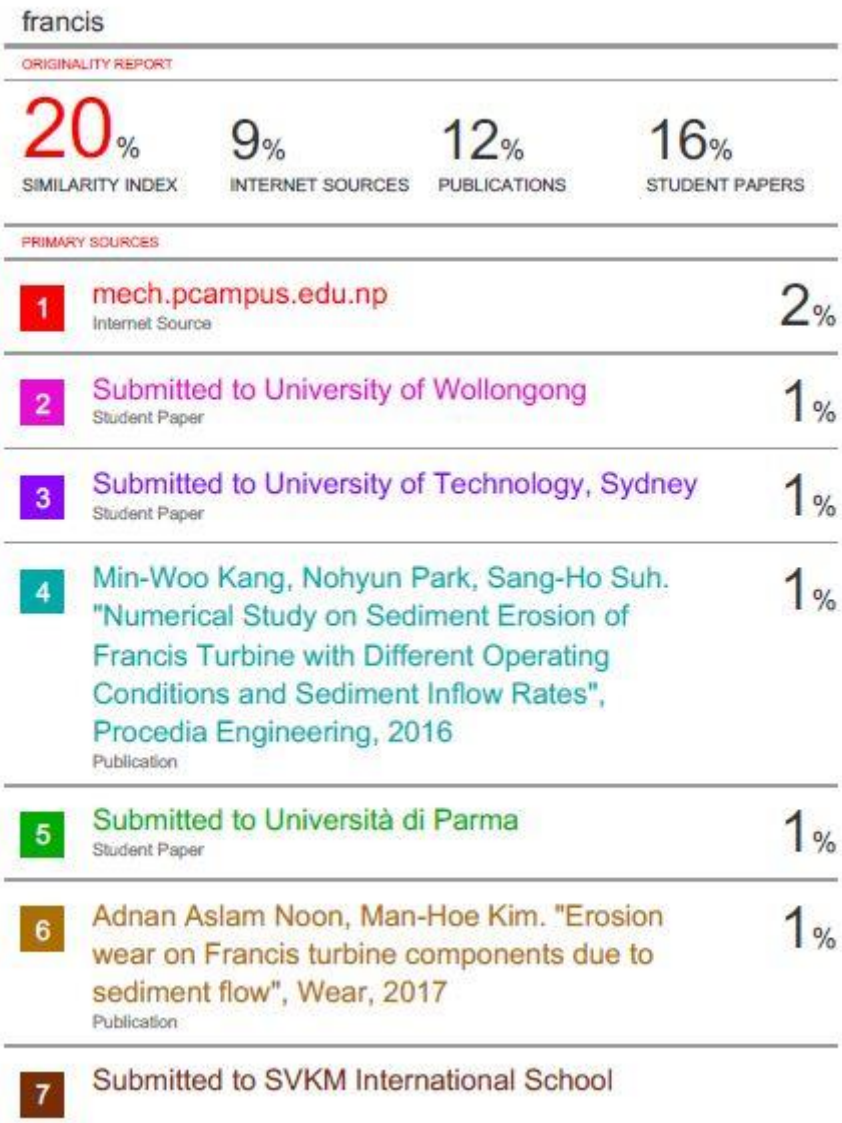

francis

ORIGINALITY REPORT

20%	9%	12%	16%
SIMILARITY INDEX	INTERNET SOURCES	PUBLICATIONS	STUDENT PAPERS

PRIMARY SOURCES

1	mech.pcampus.edu.np Internet Source	2%
2	Submitted to University of Wollongong Student Paper	1%
3	Submitted to University of Technology, Sydney Student Paper	1%
4	Min-Woo Kang, Nohyun Park, Sang-Ho Suh. "Numerical Study on Sediment Erosion of Francis Turbine with Different Operating Conditions and Sediment Inflow Rates", Procedia Engineering, 2016 Publication	1%
5	Submitted to Università di Parma Student Paper	1%
6	Adnan Aslam Noon, Man-Hoe Kim. "Erosion wear on Francis turbine components due to sediment flow", Wear, 2017 Publication	1%
7	Submitted to SVKM International School	

	Student Paper	<1%
8	brage.bibsys.no Internet Source	<1%
9	Submitted to Universiti Tenaga Nasional Student Paper	<1%
10	asmedigitalcollection.asme.org Internet Source	<1%
11	www.mdpi.com Internet Source	<1%
12	Paloma Pineda, Alfredo Iranzo. "Analysis of sand-loaded air flow erosion in heritage sites by Computational Fluid Dynamics: Method and damage prediction", Journal of Cultural Heritage, 2017 Publication	<1%
13	www.tandfonline.com Internet Source	<1%
14	mafiadoc.com Internet Source	<1%
15	Submitted to Middle East Technical University Student Paper	<1%
16	Submitted to University of Northumbria at Newcastle Student Paper	<1%